PB2000-101762

FATIGUE CRACK MODELING IN BRIDGE DECK CONNECTION DETAILS

Final Report

SPR 380

by

Robert K. Paasch
and
Anthony H. DePiero
Department of Mechanical Engineering
Oregon State University
Corvallis, Oregon 97331

for

Oregon Department of Transportation
Research Group
200 Hawthorne SE, Suite B-240
Salem, OR 97301-5192

and

Federal Highway Administration
400 Seventh Street SW
Washington, DC 20590

December 1999

REPRODUCED BY: NTIS
U.S. Department of Commerce
National Technical Information Service
Springfield, Virginia 22161

1. Report No.	2. Government Accession No.	3. Recipient's Catalog No.
FHWA-OR-RD-00-08		

4. Title and Subtitle	5. Report Date
Fatigue Crack Modeling in Bridge Deck Connection Details	December 1999
	6. Performing Organization Code
7. Author(s)	8. Performing Organization Report No.
Robert K. Paasch and Anthony H. DePiero Department of Mechanical Engineering Oregon State University, Corvallis, OR 97331	
9. Performing Organization Name and Address	10. Work Unit No. (TRAIS)
Oregon Department of Transportation Research Group 200 Hawthorne SE, Suite B-240 Salem, Oregon 97301-5192	11. Contract or Grant No. SPR 380
12. Sponsoring Agency Name and Address	13. Type of Report and Period Covered
Oregon Department of Transportation Research Group 200 Hawthorne SE, Suite B-240 Salem, Oregon 97301-5192 and Federal Highway Administration 400 Seventh Street SW Washington, D.C. 20590	Final Report
	14. Sponsoring Agency Code

15. Supplementary Notes

16. Abstract

Many steel bridges built prior to 1960 have bridge deck connections that are subject to high cycle fatigue. These connections may be nearing their fatigue limit and will require increased inspection and repair over the next 10 - 20 years. Current inspection and repair are very expensive and only address those details which contain visible cracks. The goal of this research was to develop a methodology to identify problem details – those which are nearing the end of their serviceable life, but may not yet contain visible cracks. One Oregon bridge on Interstate 5 with this problem was studied to assess the loading conditions and fatigue crack growth rate for the connection details. The objective was to use the analysis from this bridge to develop a predictive model of connection detail fatigue life, which could be applied to other bridges. Such a model could be used to guide the inspection and repair process, significantly reducing costs.

Finite element modeling methods were used to characterize the structure, and fracture mechanics was used to estimate the fatigue life of the connection details. Fatigue life estimates were found to be very conservative, and results suggested that additional field validation work would be necessary to quantify other forces on the connection details. The project resulted in a low-cost field identification methodology to identify problem details. In addition, five retrofit strategies were examined and several recommendations were made to improve the fatigue-limit estimates.

17. Key Words	18. Distribution Statement
fatigue crack, high cycle fatigue, truss flooring connection, bridge deck connection, finite element modeling	Copies available from NTIS

19. Security Classification (of this report)	20. Security Classification (of this page)	21. No. of Pages	22. Price
unclassified	unclassified	67	

Technical Report Form DOT F 1700.7 (8-72) Reproduction of completed page authorized

SI* (MODERN METRIC) CONVERSION FACTORS

APPROXIMATE CONVERSIONS TO SI UNITS

Symbol	When You Know	Multiply By	To Find	Symbol
		LENGTH		
In	Inches	25.4	millimeters	mm
Ft	Feet	0.305	meters	m
yd	Yards	0.914	meters	m
mi	Miles	1.61	kilometers	km
		AREA		
in^2	square inches	645.2	millimeters squared	mm^2
ft^2	square feet	0.093	meters squared	m^2
yd^2	square yards	0.836	meters squared	m^2
ac	Acres	0.405	hectares	ha
mi^2	square miles	2.59	kilometers squared	km^2
		VOLUME		
fl oz	fluid ounces	29.57	milliliters	mL
gal	gallons	3.785	liters	L
ft^3	cubic feet	0.028	meters cubed	m^3
yd^3	cubic yards	0.765	meters cubed	m^3
NOTE: Volumes greater than 1000 L shall be shown in m^3.				
		MASS		
oz	ounces	28.35	grams	g
lb	pounds	0.454	kilograms	kg
T	short tons (2000 lb)	0.907	megagrams	Mg
		TEMPERATURE (exact)		
°F	Fahrenheit temperature	5(F-32)/9	Celsius temperature	°C

APPROXIMATE CONVERSIONS FROM SI UNITS

Symbol	When You Know	Multiply By	To Find	Symbol
		LENGTH		
mm	millimeters	0.039	inches	in
m	meters	3.28	feet	ft
m	meters	1.09	yards	yd
km	kilometers	0.621	miles	mi
		AREA		
mm^2	millimeters squared	0.0016	square inches	in^2
m^2	meters squared	10.764	square feet	ft^2
ha	hectares	2.47	acres	ac
km^2	kilometers squared	0.386	square miles	mi^2
		VOLUME		
mL	milliliters	0.034	fluid ounces	fl oz
L	liters	0.264	gallons	gal
m^3	meters cubed	35.315	cubic feet	ft^3
m^3	meters cubed	1.308	cubic yards	yd^3
		MASS		
g	grams	0.035	ounces	oz
kg	kilograms	2.205	pounds	lb
Mg	megagrams	1.102	short tons (2000 lb)	T
		TEMPERATURE (exact)		
°C	Celsius temperature	1.8 + 32	Fahrenheit	°F

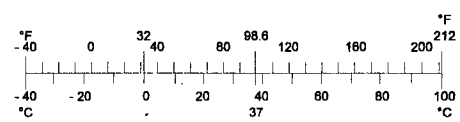

* SI is the symbol for the International System of Measurement

(4-7-94 jbp)

ACKNOWLEDGEMENTS

The author would like to thank the members of the ODOT Research Group (Marty Laylor and Alan Kirk) and the Technical Advisory Committee for this project, for their advice and assistance in the preparation of this report.

DISCLAIMER

This document is disseminated under the sponsorship of the Oregon Department of Transportation and the United States Department of Transportation in the interest of information exchange. The State of Oregon and the United States Government assume no liability of its contents or use thereof.

The contents of this report reflect the views of the authors, who are responsible for the facts and accuracy of the data presented herein. The contents do not necessarily reflect the official policies of the Oregon Department of Transportation or the United States Department of Transportation.

The State of Oregon and the United States Government do not endorse products of manufacturers. Trademarks or manufacturers' names appear herein only because they are considered essential to the object of this document.

This report does not constitute a standard, specification, or regulation.

PROTECTED UNDER INTERNATIONAL COPYRIGHT
ALL RIGHTS RESERVED.
NATIONAL TECHNICAL INFORMATION SERVICE
U.S. DEPARTMENT OF COMMERCE

Reproduced from
best available copy.

HIGH CYCLE FATIGUE CRACKS IN BRIDGE DECK CONNECTION DETAILS

TABLE OF CONTENTS

1.0 INTRODUCTION 1

2.0 PROBLEM SPECIFICATION 3

3.0 BACKGROUND AND THEORY 7

3.1 BACKGROUND 7
3.1.1 Wilson Studies 7
3.1.2 Colorado Study 8
3.1.3 NCHRP Study 8
3.2 FINITE ELEMENT ANALYSIS (FEA) 8
3.2.1 Global FEA Modeling 9
3.2.2 2D FEA Modeling 9
3.2.3 3D FEA Modeling 9
3.3 FATIGUE 10
3.3.1 Strain-Life Fatigue Analysis 10
3.3.2 Stress-Life Fatigue Analysis 11
3.3.3 Linear-Elastic Fracture Mechanics 12

4.0 LOADING ANALYSIS 15

4.1 STRINGER LOADING ANALYSIS 15
4.2 GLOBAL FEA MODEL 17
4.2.1 Reinforced Concrete Deck Analysis 17
4.2.2 Model Validation 18
4.3 RESULTS 21

5.0 DEFLECTION AND STRESS ANALYSIS 25

5.1 CLIP ANGLE DEFLECTION AND STRESS ANALYSIS 25
5.2 2D FEA MODEL 29
5.3 3D FEA MODEL 30
5.3.1 Element Density 31
5.3.2 Boundary Conditions 31
5.3.3 Rivet Pre-load and Friction 31
5.3.4 Clip Angle Thickness 32
5.4 RESULTS 32

6.0 FATIGUE ANALYSIS 39

6.1 STRESS-LIFE 39
6.2 LINEAR-ELASTIC FRACTURE MECHANICS (LEFM) 41
6.3 REMAINING FATIGUE LIFE 42
6.4 RESULTS 43

7.0 IDENTIFICATION METHODOLOGY 45

8.0 RETROFIT STRATEGIES 49

9.0 SUMMARY, CONCLUSIONS AND FUTURE WORK 53
10.0 REFERENCES 55

APPENDICES

APPENDIX A: STRINGER LOADING ANALYSIS
APPENDIX B: GLOBAL FEA MODEL
APPENDIX C: REINFORCED CONCRETE DECK ANALYSIS
APPENDIX D: CLIP ANGLE DEFLECTION ANALYSIS
APPENDIX E: CLIP ANGLE STRESS ANALYSIS
APPENDIX F: 2D FEA MODEL
APPENDIX G: 3D FEA MODEL
APPENDIX H: STRESS LIFE
APPENDIX I: LINEAR ELASTIC FRACTURE MECHANICS
APPENDIX J: IDENTIFICATION METHODOLOGY

NOTE: These Appendices may be obtained from the Oregon Department of Transportation Research Group, 200 Hawthorne Ave. SE, Suite B-240, Salem, OR 97301-5192. Telephone: 503-986-2700.

List of Tables

Table 5.1: Comparison of Interior Panel Clip Angle Deflections (in.) from Each Analysis Method.....34
Table 5.2: Comparison of Interior Panel Clip Angle Maximum Stress Range (ksi) Results.....37
Table 5.3: Clip Angle Stress Range Results from the 3D FEA Model for Different Locations 37
Table 6.1: Estimated Remaining Life (Years) of the Different Clip Angles - Stress-Life Fatigue Analysis.....43
Table 6.2: Estimated Remaining Life (Years) of the Different Clip Angles - Linear-Elastic Fracture Mechanics.....44
Table 8.1: Effectiveness of the Five Retrofit Strategies Investigated 51

List of Figures

Figure 1.1: Flow chart of the project phases 2
Figure 2.1: Diagram of one span of the southbound structure of the Winchester Bridge without the six inch concrete deck 3
Figure 2.2: Typical stringer - to - floor beam connection detail assembly 4
Figure 2.3: Winchester Bridge clip angle used in the stringer - to - floor beam assemblies 4
Figure 2.4: Clip angle with a typical fatigue crack 5
Figure 3.1: Three modes of crack displacement 13
Figure 4.1: Suggested standard fatigue truck outlined in the NCHRP Report 299 15
Figure 4.2: Top view diagram of the three stringers that are assumed to carry the axle load in the stringer loading analysis 16
Figure 4.3: Diagram of the loading and boundary conditions used in the stringer loading analysis 16
Figure 4.4: Location of strain gauges installed on three stringers and two floor beams on the northbound structure of the Winchester Bridge 19
Figure 4.5: Stringer stress ranges from the global FEA model and those measured experimentally, loaded with a known truck weight 20
Figure 4.6: Stringer stress ranges from the global FEA model and those measured experimentally, under random traffic loading 20
Figure 4.7: Stringer loads for the northbound structure for both the stringer loading analysis and the global FEA model 21
Figure 4.8: Stringer loads for the southbound structure for both the stringer loading analysis and the global FEA model 22
Figure 4.9: Load on the second from middle stringer vs. the deck thickness from the global FEA model 23
Figure 5.1: Stringer model, illustrating loading and boundary conditions 25
Figure 5.2: Top of the floor beam leg of the clip angle modeled as a cantilever beam 26
Figure 5.3: Diagram of clip angle showing the center of rotation and the relationship of F_R and M_o 27
Figure 5.4: 2D FEA model of the top of the clip angle illustrating size dimensions, boundary conditions, and loading 29
Figure 5.5: Exaggerated deflection plot from the 2D FEA model of an interior panel clip angle 33
Figure 5.6: Exaggerated deflection plot from the 3D FEA model of an interior panel clip angle 33
Figure 5.7: Fringe plot of the maximum principal stress for an interior panel clip angle from the 2D FEA model 35
Figure 5.9: Fringe plot of the maximum principal stress from the 3D FEA model using the fixed top flange model of the floor beam 36
Figure 7.1: Load on the second-from-middle stringer vs. the stringer spacing 46
Figure 8.1: Retrofit strategy #2 used to replace damaged clip angles on the Winchester Bridge in 1994 50
Figure 8.2: Diagram of the retrofit strategy #5; geometric stiffening 51

1.0 INTRODUCTION

The Oregon Department of Transportation (ODOT) is responsible for approximately 320 steel bridges, many of which have flooring system connection details that are prone to fatigue. The majority of these bridges, which were built prior to 1960, have details nearing the end of their fatigue life and will require increased inspection and repair over the next 10 to 20 years. Bridges on major routes will require added attention, since they can experience as many as 1 to 5 million significant load cycles per year. Some of these bridges have over 1,000 connection details, making the cost of inspection and repair very expensive. To date, details with fatigue cracks have been found in over 20 structures.

The need exists to accurately assess the loading conditions and fatigue crack growth rate for the connection details and to develop a low-cost field identification methodology to identify problem details. The current procedure is to repair only those connection details that contain visible fatigue cracks. Other connection details remain in service even though they may be nearing the end of their serviceable life. A more economic repair procedure could be implemented if there were detailed knowledge about which details were nearing the end of their fatigue life. Thus the need to quantify the fatigue condition of the connection details is driven by the desire to limit inspection costs and to repair or replace only details with potential problems.

The goal of this research was to accurately assess the loading conditions and the fatigue crack growth rate for the connection details of a specific bridge, the Winchester Bridge on Interstate 5 in Roseburg, Oregon. Using the analysis from one bridge, there was an expectation that the procedure, and to some degree, the results, could be applied to other bridges.

The research design is shown on the flowchart in Figure 1.1. Chapter 2 discusses the problem specifications and describes the specific bridge for study. Background information on fatigue, finite element analysis and fracture is presented in Chapter 3. Chapter 4, Loading Analysis, addresses the two analysis methods used to determine the loading on the stringers (beams attached to connection details). In Chapter 5, Stress and Deflection Analysis, the deflections and stress ranges of the connection details are quantified. Detailed finite element models are used extensively in the loading analysis and the deflection and stress analysis. Hand calculations are used to gain insight into the process and guide the development of the finite element models. Experimental data is used to validate the analysis. Chapter 6, Fatigue Analysis, includes reviews of the two methods used for estimating the remaining life of a connection detail. The development of a low-cost field identification methodology to identify problem connection details is discussed in Chapter 7. In Chapter 8, results are presented from the investigation of five retrofit strategies. The research project is summarized in Chapter 9.

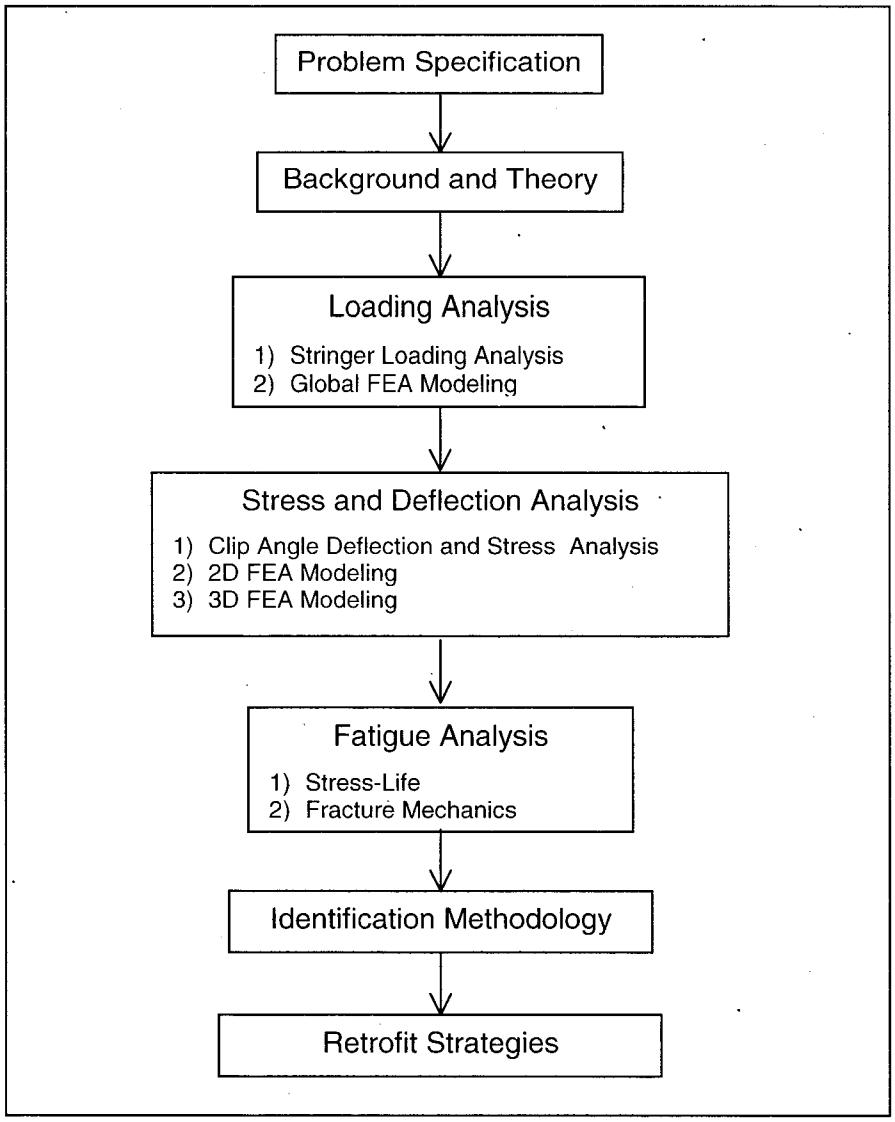

Figure 1.1: Flow chart of the project phases

2.0 PROBLEM SPECIFICATION

The Winchester Bridge is a typical steel deck truss bridge under the responsibility of ODOT. The bridge was selected for this study because it has experienced high cycle fatigue problems in its flooring system connection details. The Winchester Bridge is located on Interstate 5, five miles north of Roseburg, Oregon, and spans the North Fork of the Umpqua River. The bridge has separate north- and southbound structures that were constructed in 1953 and 1963, respectively. The two structures are very similar in their construction. Each structure is made of six, 140-foot (42.7 m) steel deck truss spans. Figure 2.1 illustrates one span of the southbound structure without showing the reinforced concrete deck. The spans are separated by expansion joints, making them independent of one another.

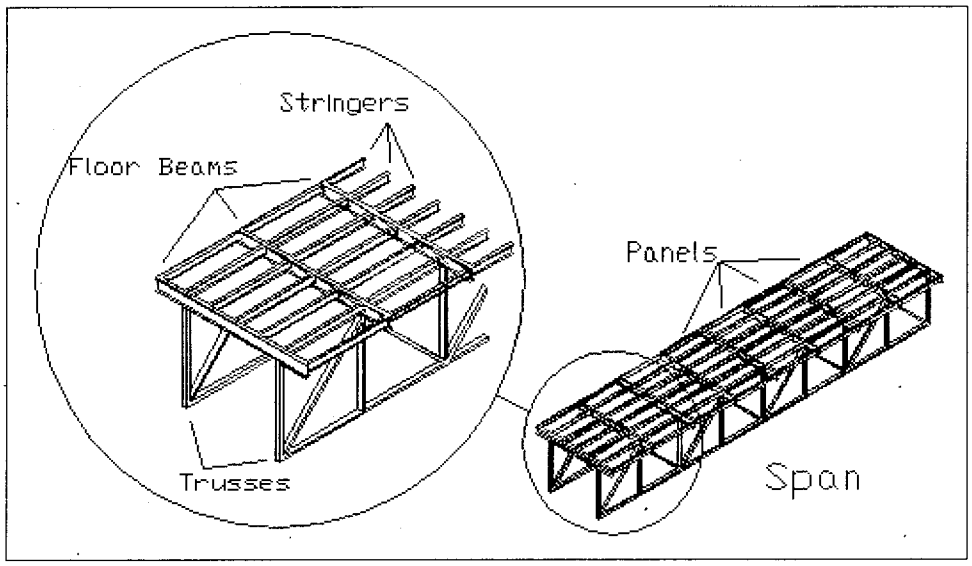

Figure 2.1: Diagram of one span of the southbound structure of the Winchester Bridge without the six inch concrete deck

Each span is made up of a pair of steel trusses whose center lines are 20 feet (6.1 m) apart. Each pair of trusses supports nine laterally oriented floor beams that are 17½ feet (5.3 m) apart. The sections between the floor beams are called "panels". The northbound structure has five stringers in each panel running between the floor beams. The southbound structure has seven stringers in each panel. A six-inch (150 mm) thick reinforced concrete deck lies on top and is supported by the floor beams and stringers. The north- and southbound structures have slightly different size floor beams and stringers. In the northbound structure, the floor beams are W24 x 76 wide-flange steel beams and the stringers are W18 x 50 wide-flange steel beams. In the southbound structure, the floor beams are W27 x 84 wide-flange steel beams and the stringers are W18 x 45

wide-flange steel beams. Figure 2.2 shows a typical connection detail assembly of a stringer to a floor beam.

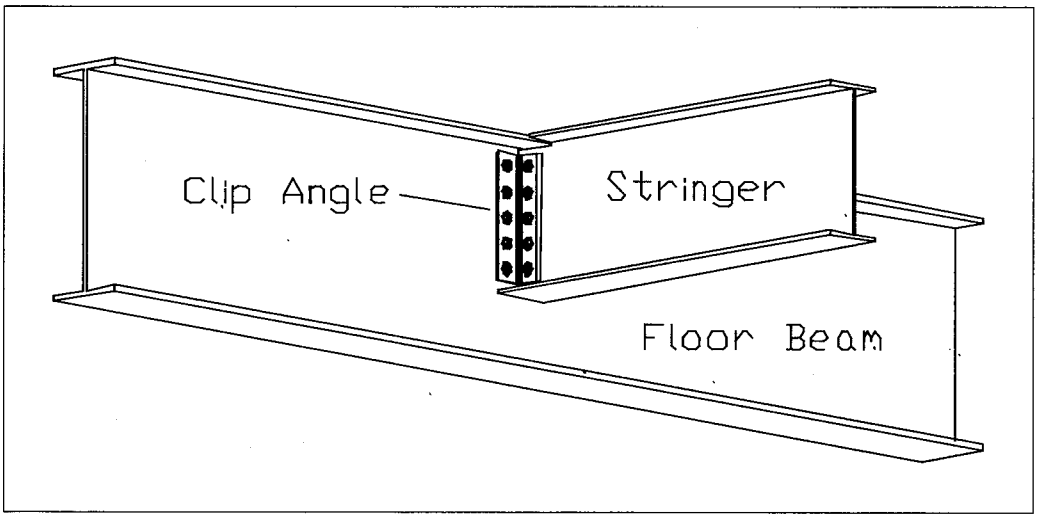

Figure 2.2: Typical stringer - to - floor beam connection detail assembly

The clip angles are connected to the stringers and floor beams using 7/8 inch (22 mm) diameter rivets. Rivet holes are positioned 1.5 inches (38 mm) from the edges and spaced 3 inches (75 mm) apart on center. The clip angle's primary function is to transmit the shear from the stringer to the floor beam. Figure 2.3 is a clip angle used in the stringer - to - floor beam assembly on the Winchester Bridge.

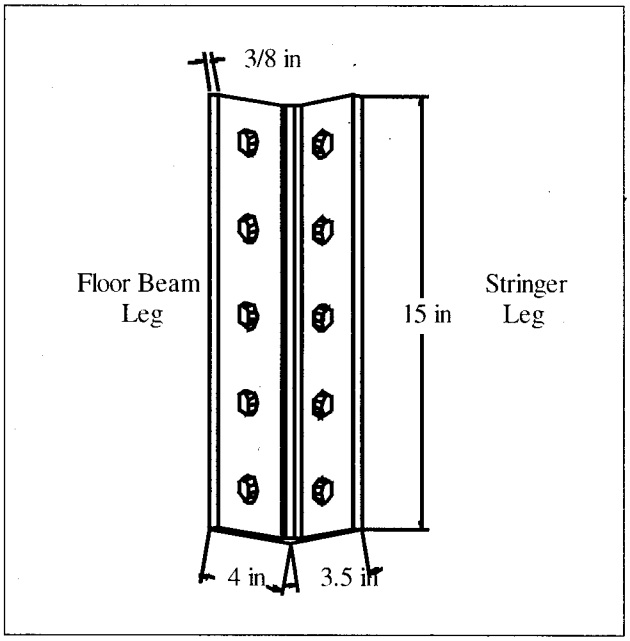

Figure 2.3: Winchester Bridge clip angle used in the stringer - to - floor beam assemblies

Since the angles are riveted to both the stringer and floor beam, they are subjected to flexural stresses caused by the vertical deflection of the stringer under wheel loads. As the stringer deflects, the rotation of the end of the stringer subjects the connection detail to a flexural moment over time, and this flexural moment leads to fatigue cracking in the clip angles.

Fatigue cracks as long as 4 inches (100 mm) have been found in the clip angles that connect the stringers to the floor beams on the Winchester Bridge. The fatigue cracks were typically found in the clip angles connecting the stringers to the floor beams at the ends of the spans, although some were found in interior clip angles. The cracks were located at the corner of the clip angle running vertically from the top of the clip angle down. The fracture surface of the cracks was usually oriented at about a 45 degree angle to the legs of the clip angle. Figure 2.4 illustrates a clip angle with a typical fatigue crack.

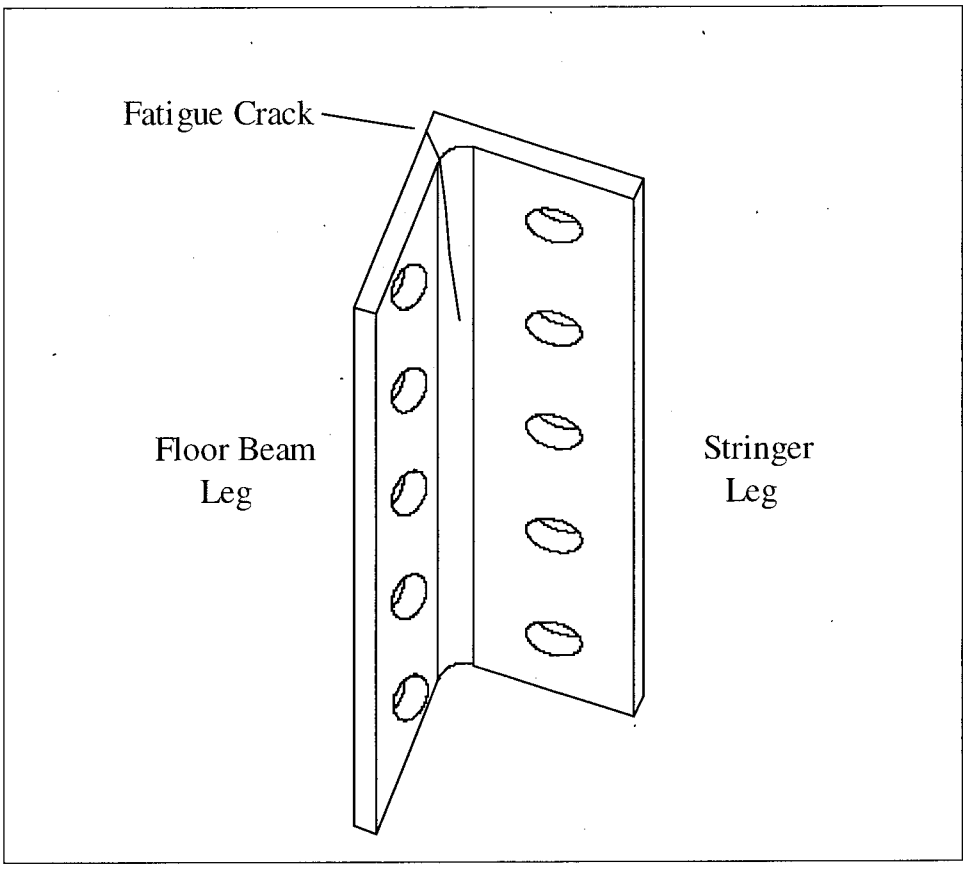

Figure 2.4: Clip angle with a typical fatigue crack

In 1994 repairs were conducted on both the north- and southbound structures of the Winchester Bridge. Thirteen cracked clip angles were replaced on the southbound structure at a cost of $16,384. Similar work was performed on the northbound structure at a cost of $16,296.

The north- and southbound structures of the Winchester Bridge were logical choices on which to perform a detailed analysis. The structures are typical steel deck truss bridges that have had significant fatigue problems and also experience a high number of load cycles per year. They also serve as an important link along the I-5 corridor in providing safe and efficient movement of people and goods through the state.

3.0 BACKGROUND AND THEORY

This section focuses on previous research and theories associated with fatigue analysis. The examination of research performed on similar projects can give insight and help in understanding the problem currently being studied:

- The connection angles examined in a railway bridge connection angles study performed by Wilson of the University of Illinois were very similar to the clip angles used on the Winchester Bridge (*Wilson 1940*).
- In Colorado, a finite element analysis and field testing were performed on a bridge over the South Platte River near Commerce City (*Cao, et al. 1996*).
- The National Cooperative Highway Research Program (NCHRP) Report 299, *Fatigue Evaluation Procedures for Steel Bridges*, contains comprehensive fatigue evaluation procedures developed to guide the fatigue evaluation of existing bridges (*Moses, et al. 1987*).

These three studies are discussed in the following section.

3.1 BACKGROUND

3.1.1 Wilson Studies

Fatigue in bridges has been a concern to the transportation community for many years. In the late 1930's Wilson and Coombe of the University of Illinois performed studies of connection angles for stringers on railway bridges (*Wilson and Coombe 1939, and Wilson 1940*). Computational analysis and fatigue testing were performed for the studies.

The connection details that Wilson examined experienced flexural stresses due to deformation of the bridge. Two distinct actions contributed to those flexural stresses. The first was the lengthening of the bottom chord of the truss when a train was traveling on the bridge. The stringers did not experience a corresponding change in length; and since the floor beams are connected to both bottom chord and the stringers, an axial force was produced and transmitted through the connection angles. One stress cycle was completed for each train passage.

The second action was the vertical deflection of the stringer under each set of wheels. The deflection rotated the end of the stringer and subjected the connection detail to a flexural moment. Stress cycles from this action were repeated for the passage of each car.

Wilson concluded that, because the stress in a flexural member varies as the square of the length, the stress state is much worse for connection details with short stiff legs than those with longer more flexible legs (*Wilson 1940*).

In a separate study nine connection details with three different configurations were fatigue tested by repeatedly applying axial loads. The tests were designed to find the fatigue strengths of both the connection angles and the rivets (*Wilson and Coombe 1939*).

3.1.2 Colorado Study

The purpose of this study on the reinforced concrete bridge decks on Colorado State Route 224 was to determine whether the top transverse reinforcing bars in the deck were necessary to sustain the negative bending moments and the tensile stresses seen in the top of the deck over the girders. Since the top transverse reinforcing bars were most susceptible to corrosion from deicing chemicals, there was an interest to see if they could be eliminated, without compromising the structural integrity of the bridge deck (*Cao, et al. 1996*).

A finite element model was used in conjunction with experimental testing to determine the stress of the deck over the girders. The concrete deck and the girders were modeled. The concrete deck in the vicinity of the load points was modeled using two layers of solid elements. The girders were modeled using 3D beam elements. Rigid beam elements were used to connect the nodes on the bottom of the deck to the centroid of the girders. In areas away from the load points, equivalent beam elements were used to model the combination of the deck and the girders (*Cao, et al. 1996*).

3.1.3 NCHRP Study

A substantial amount of research has been done to develop fatigue evaluation procedures for bridges. NCHRP Report 299, *Fatigue Evaluation Procedures for Steel Bridges,* outlines procedures for evaluating fatigue conditions of existing steel bridges (*Moses, et al. 1987*). The report discusses several loading issues, such as the proposed standard fatigue truck, impact, truck superposition, and cycles per truck passage. The report contains methods for calculating moment ranges, stress ranges and the remaining fatigue life. Options are presented for different levels of effort that reduce uncertainties and improve predictions of remaining life. The evaluation procedures provide an effective guide to developing the analysis methods used on this research project.

3.2 FINITE ELEMENT ANALYSIS (FEA)

In addition to previous research, an understanding and use of finite element analysis (FEA) and fatigue theory are very important. This section discusses FEA and the FEA modeling tools used in this research project. In Section 3.3 three methods of fatigue analysis are reviewed.

The finite element method, which was introduced in the late 1950's, is a computer simulation model used to perform computational mechanics. With this model, the component of interest is first divided up into many small boxes or elements. The elements can have irregular shapes and conform closely to the shape of the component being modeled. The collection of elements forms a three-dimensional grid or mesh and makes the object look as if it were made of small building blocks. Nodes are points in the mesh where elements are connected. Discrete equations are used

to mathematically couple adjacent nodes of the mesh to one another. Although the equations couple only adjacent nodes, they are derived from global balance laws. The following sections discuss the finite element method modeling tools that are used in the global FEA model, the 2D FEA model, and the 3D FEA model.

3.2.1 Global FEA Modeling

COSMOS/M was used to perform the finite element macro modeling in this study. COSMOS/M is a modular, self-contained finite element system developed by Structural Research and Analysis Corporation (*COSMOS/M User's Guide 1992*). The module GEOSTAR was used as the mesh generator and post-processor. The STAR module was used for the linear static analysis of the deck structure. Other modules are available with a variety of different modeling capabilities.

3.2.2 2D FEA Modeling

The 2D modeling in this study was performed using codes developed by the Methods Development Group at Lawrence Livermore National Laboratory (LLNL). MAZE was used to generate the mesh. It was developed as a mesh generator for the LLNL family of 2D FEA codes (*Hallquist 1983*).

NIKE2D was used to perform the analysis. This program is a nonlinear, implicit, 2D finite element code for solid mechanics. It uses a variety of elastic and inelastic material models. It has slide line algorithms that permit gaps, frictional sliding, and single surface contact along material interfaces (*Engelmann 1991*).

ORION was used to view the results generated by NIKE2D. It is an interactive color post-processor developed to view the results of the 2D FEA codes at LLNL (*Hallquist and Levatin 1992*).

3.2.3 3D FEA Modeling

Mesh generation for the 3D FEA model in this study was performed using INGRID and later using TrueGrid. INGRID is a generalized 3D finite element mesh generator developed by the Methods Development Group at LLNL. It has the capability of generating complex geometrical models of nonlinear systems with beam; shell, and hexahedral elements (*Christon and Dovey 1992*).

TrueGrid is a highly interactive mesh generator for a wide range of 3D FEA codes. It is similar to INGRID and will generate complex meshes using beam, shell, and hexahedral elements. It was developed by XYZ Scientific Applications, Inc. (*TrueGrid User's Manual 1995*).

The FEA codes used for the 3D modeling were NIKE3D and LS-NIKE3D. NIKE3D is a nonlinear, implicit, 3D finite element code for solid and structural mechanics. NIKE3D uses beam, shell, and hexahedral elements and a variety of elastic and inelastic material models. It has contact-impact algorithms that permit gaps, frictional sliding, and mesh discontinuities along material interfaces. NIKE3D was originally developed by John Hallquist of the Methods

Development Group at LLNL. The development was continued by Bradley Maker and Robert Ferencz (*Maker 1991*).

LS-NIKE3D is an implicit, finite-deformation, finite element code for analyzing the static and dynamic response of three-dimensional solids. LS-NIKE3D was developed by Livermore Software Technology Corporation (LSTC) using the NIKE3D code developed at LLNL. Major developments made in the contact algorithms and the linear equation solving technology have made LS-NIKE3D robust and efficient (*LS-NIKE3D User's Manual 1996*).

The post processor used to view the results generated by the 3D FEA code was LS-TAURUS. LS-TAURUS is a highly interactive post-processor developed by LSTC to display results of LLNL and LSTC families of 3D FEA codes. It originated from LLNL post-processors developed by John O. Hallquist (*LS-TAURUS User's Manual 1995*).

3.3 FATIGUE

Fatigue is the process responsible for premature failure or damage of components subjected to repeated loading (*Bannantine and Comer 1990*). Fatigue is considered low cycle if the number of load cycles to failure is less than 1000 cycles, and high cycle if the number of load cycles to failure is more than 1000 cycles. Fatigue is often divided into two phases; crack initiation and crack propagation. Crack initiation is the phase where a crack is formed, usually around an inclusion or other defect. Crack propagation occurs when the crack increases in length with subsequent load cycles. The boundary between the two phases is often very difficult to determine.

Three general methods of fatigue analysis are used in structural analysis and design. They are strain-life, stress-life, and linear-elastic fracture mechanics. Each method has strengths and weaknesses, and one or another may be more appropriate for different classes of problems. Knowledge about the material, loading, geometry, whether the fatigue is low or high cycle, and whether the phase of interest is initiation and/or propagation is helpful in determining which method is most appropriate.

3.3.1 Strain-Life Fatigue Analysis

The strain-life method uses true strain to predict the number of cycles to failure. When components are under high load and/or have critical locations (notches), the stress-strain relationship is no longer linearly related. In these situations the plastic strain becomes a significant part of the deformation. Since the primary mechanism in fatigue is plastic deformation, an elastic model is not appropriate.

The strain-life method uses the level of deformation explicitly, and it is more appropriate for cases with high plastic deformation. These types of cases fall into the low cycle fatigue category. The strain-life method compares the true strain range to a strain versus fatigue life curve. One weakness of this method is that finding true strain in areas of discontinuities can be very difficult.

More experimental data are needed to account for surface finish, surface treatment, loading, and other modifying parameters.

3.3.2 Stress-Life Fatigue Analysis

The stress-life method uses the alternating stress amplitude to predict the number of cycles to failure. This method is based on comparing the stress amplitude to a stress versus fatigue life curve (S-N diagram). The S-N curves are based on empirical formulas derived from experimental data. The stress-life method is generally only used for high cycle fatigue, because under low cycle fatigue the stress-strain relationship becomes nonlinear.

For many metals (including steel) there exists a region of infinite life, where fatigue problems will not develop if the stress amplitude is below a threshold value. This threshold value is called the endurance limit (S_e) (*Shigley and Mischke 1989*). In many materials, the endurance limit has been related to the ultimate tensile strength (S_{UT}) through experimental testing. The ideal endurance limit (S_e') for steels with an ultimate tensile strength less than 200 ksi (1,373 MPa) is roughly $0.5 \cdot S_{UT}$ (*Shigley and Mischke 1989*). The ideal endurance limit is calculated in a laboratory under carefully controlled conditions. The ideal endurance limit is then related to the actual endurance limit by applying factors that account for differences in surface finish, surface treatments, size, temperature, loading, and other environment factors (*Bannantine and Comer 1990*).

The S-N diagram is a log scale plot of the fully reversed stress amplitude (stress cycles from -S to +S) versus the number of stress cycles to failure. For steel, the S-N diagram is generally plotted by connecting a line from the fatigue strength at 10^3 cycles to the endurance limit (S_e) at 10^6 cycles. The fatigue strength at 10^3 is only slightly less than the S_{UT} and is taken to be $0.9 \cdot S_{UT}$ (*Shigley and Mischke 1989*).

For the cases where the stress mean is not zero, an equivalent stress amplitude (S) must be calculated from the mean stress (σ_m) and the stress amplitude (σ_a). There are two relationships that tend to bracket the test data. They are the Goodman and Gerber relationships. The equations are shown below. The Goodman relationship is the more conservative of the two and is often used for that reason (*Bannantine and Comer 1990*).

$$S = \frac{\sigma_a}{1 - \frac{\sigma_m}{S_{UT}}} \qquad \textbf{(3-1)}$$

Goodman Relationship

$$S = \frac{\sigma_a}{1 - \left(\frac{\sigma_m}{S_{UT}}\right)^2} \tag{3-2}$$

Gerber Relationship

The endurance limit is based on a constant amplitude alternating stress. There are many instances where the stress amplitude is variable. In these cases, a method for calculating cumulative damage is used to find an effective alternating stress. A root mean cubed method is often used to estimate cumulative damage (*Moses, et al. 1987*). The individual stress range values are first cubed, an average is taken, and then the cube root of the average is determined. The result is an effective stress range value that is larger than the value obtained from the arithmetic average, because cubing the stress range values increases the emphasis on the large values in the distribution. If the alternating stress is not fully reversed, an equivalent stress amplitude is then calculated using either the Goodman or Gerber relationship.

Even though the effective stress amplitude may be less than the fatigue limit, many amplitudes may still fall above the fatigue limit. This typically results in a finite life. Distributions with as low as one stress amplitude in a thousand above the fatigue limit have still been found to exhibit a finite life (*Fisher, et al. 1983*).

One method of calculating the finite life for variable amplitude alternating stress is to extend the S-N curve beyond the constant amplitude fatigue limit (*Moses, et al. 1987*). The slope of the extension can be adjusted to reflect the distribution of cycles above the constant amplitude fatigue limit.

The stress-life method is completely empirical in nature and is limited only to cases of high cycle fatigue. It has, however, been employed for many years, and there is a considerable body of experimental evidence that has been used to derive the empirical solutions.

3.3.3 Linear-Elastic Fracture Mechanics

Linear-elastic fracture mechanics (LEFM) is an analytical method that relates the stress at a crack tip to the nominal stress field around the crack. LEFM began with Griffith's work in the 1920's. Griffith proposed a crack will propagate in brittle materials if the total energy of the system is reduced by the propagation. In the 1940's, progress continued with Irwin's work with ductile material theory. Irwin reported that the energy applied to plastic deformation must be added to the surface energy associated with the new crack surface. In the 1950's Irwin also developed equations for the local stresses near the crack tip (*Bannantine and Comer 1990*).

There are three modes describing crack displacement: Mode I, opening or tensile mode; Mode II, sliding or in-plane shear; and Mode III, tearing or anti-plane shear. Figure 3.1 shows a schematic representation of each of these three modes. For most structures Mode I is the dominant condition.

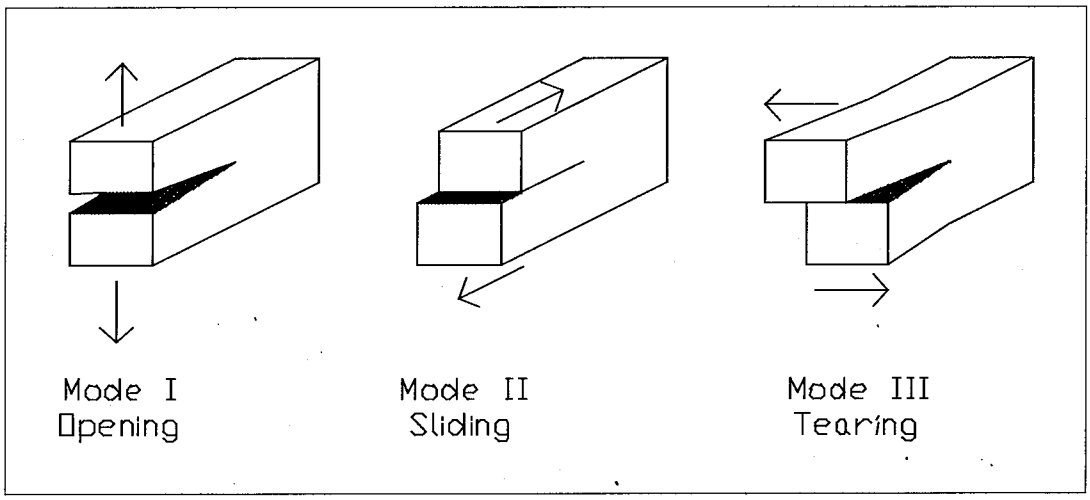

Figure 3.1: Three modes of crack displacement

With the existence of a crack, there is an infinite stress concentration at the crack tip. The stress intensity factor (K) allows the singularity to be dealt with in terms of strain energy. The stress intensity factor describes the entire stress state around the crack tip. K is a function of the nominal stress, crack length, and geometric factors. The stress intensity factor is described as follows:

$$K = F_e \cdot F_s \cdot F_w \cdot F_g \cdot \sigma \cdot \sqrt{\pi \cdot a} \qquad \textbf{(3-3)}$$

where

a is the crack length for an edge crack and half the crack length for an internal crack,

σ is the nominal tensile stress normal to the crack plane,

F_e is a factor for crack shape,

F_s is a factor to account for surface cracks,

F_w is a factor for a specimen with finite width, and

F_g is a factor for non-uniform nominal stress (*Fisher, et al. 1989*).

If the stress intensity at the crack tip reaches a critical value, the crack will begin unstable propagation. This critical stress intensity is called the fracture toughness (K_C). The fracture toughness can be used to calculate the critical crack length at which unstable propagation will occur. For Mode I crack displacement with plane strain conditions existing at the crack tip, the

fracture toughness is denoted by K_{IC}. K_{IC} values are obtained by using ASTM E-399, Test Method for Plane Strain Fracture Toughness of Metallic Materials (*Barsom and Rolfe 1987*).

There are three regions of fatigue crack growth. Region I includes the initiation stage, where the crack growth rate is small and threshold effects are important. Region II is a region of consistent and predictable crack growth rate. Region III is a region of rapid and unstable crack growth rate. Generally speaking, Region III does not contribute significantly to the fatigue life and is ignored (*Bannantine and Comer 1990*).

The stress intensity can be related to the fatigue crack growth rate as *da/dN*. When the stress field around a crack is alternating, this produces an analogous alternating stress intensity factor (ΔK). ΔK is calculated the same as K (Equation 3-3) except that σ is replaced by $\Delta\sigma$. In Region II, the slope of the log *da/dN* versus the log ΔK curve is linear, and *da/dN* and ΔK are related by the Paris equation (*Shigley and Mischke 1989*):

$$\frac{da}{dN} = C \cdot [\Delta K(a)]^M \tag{3-4}$$

where

da/dN is the crack growth rate,

ΔK is the alternating stress intensity factor,

N is the number of cycles, and

C and M are empirical constants of the material.

The fatigue life is determined by evaluating the integral:

$$N = \int_{a_i}^{a_f} \frac{1}{C \cdot [\Delta K(a)]^M} da \tag{3-5}$$

where

a_i is the initial crack size, and

a_f is the final crack size.

The final crack size is usually set as the critical crack size. The initial crack size is often set as the size of largest defect that is expected to be present. The largest defect size is often difficult to determine. The initial crack size is very important, because when the crack length is small, the crack growth rate is also very small.

4.0 LOADING ANALYSIS

This chapter describes two analysis methods used to calculate the distribution of live truck loads on the stringers. The first method – stringer loading analysis – is a linear-elastic analysis hand calculation. The second method – the global FEA model – was performed using the finite element method. A model validation analysis of the global FEA model is also discussed. The live loading results of the two analyses are also presented in Section 4.3.

For both analysis methods, the suggested standard fatigue truck, outlined in the NCHRP Report 299, was used for model loading (*Moses, et al. 1987*). Figure 4.1 shows a diagram of the standard fatigue truck. This truck was developed to represent the variety of different types and weights of trucks in actual traffic. It consists of two rear axles of 24 kips (10.9 Mg) each, and a front axle of 6 kips (2.7 Mg). The rear axles are spaced 30 feet (9.1 m) apart, while the front and the first rear axle are spaced 14 feet (4.3 m) apart. The width of each axle is 6 feet (1.8 m).

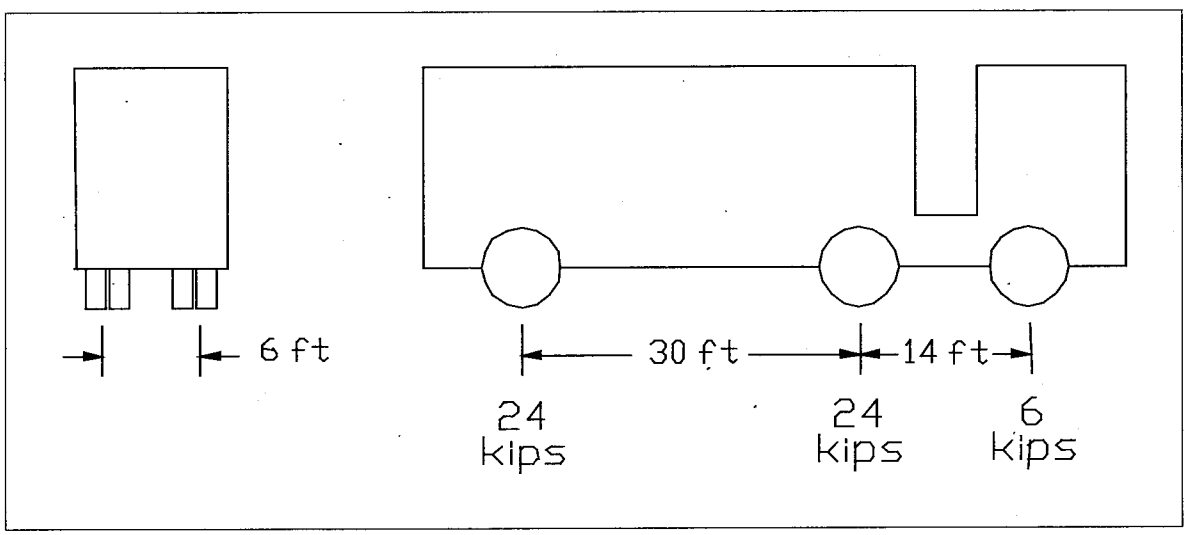

Figure 4.1: Suggested standard fatigue truck outlined in the NCHRP Report 299

4.1 STRINGER LOADING ANALYSIS

The distribution of the truck loads through the deck on the stringers is important in determining the loading on the clip angle. The loads on each stringer were calculated with one rear axle of the fatigue truck positioned longitudinally in the center of a panel over the mid-length of the stringers. Laterally, the axle was centered in the slow lane of traffic. For both the north- and southbound structures, three stringers were assumed to carry the entire weight of the axle. Those stringers were the middle stringer, the second-from-the-middle stringer, and the third-from-the-middle stringer in the slow lane. Figure 4.2 shows the location of the three stringers.

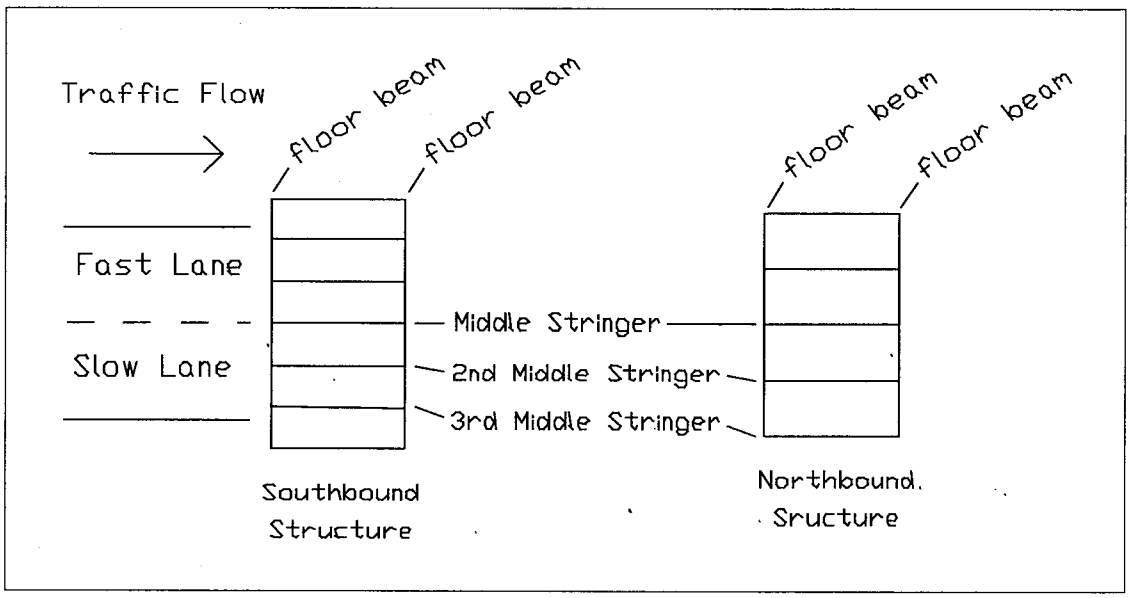

Figure 4.2: Top view diagram of the three stringers that are assumed to carry the axle load in the stringer loading analysis

Each section of the deck between the three stringers was analyzed as an independent beam, using beam tables (*Shigley and Mischke 1989*). The stringer loads were calculated as the reaction forces at the ends of the beams. Figure 4.3 shows a diagram of the loading and boundary conditions. The stringer loads for both the north- and southbound structures can be found in the results section. For details of the analysis, see Appendix A.

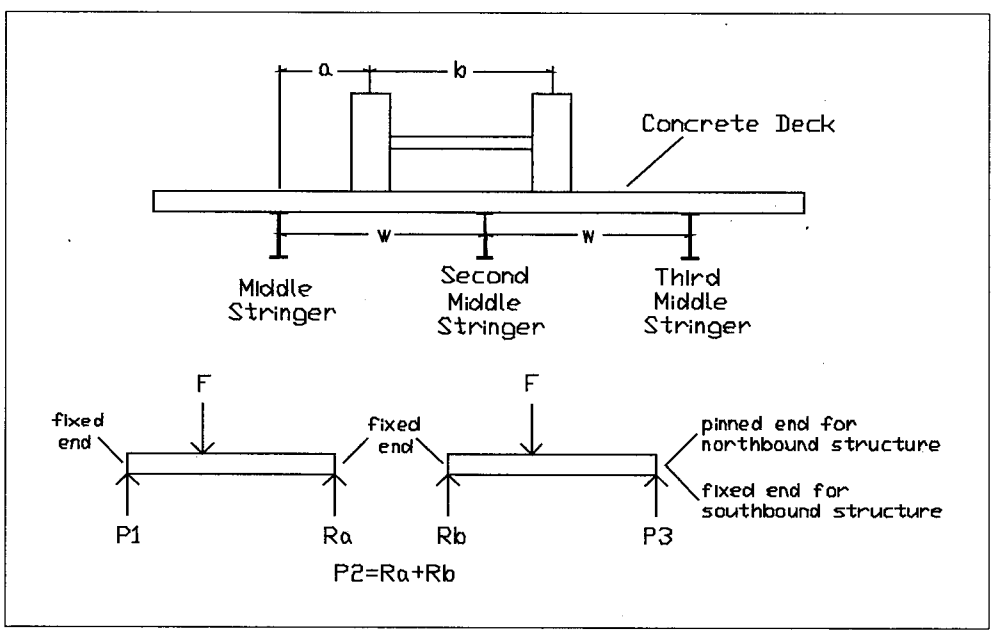

Figure 4.3: Diagram of the loading and boundary conditions used in the stringer loading analysis

4.2 GLOBAL FEA MODEL

Finite element models for both the north- and southbound structures were developed to determine the distribution of loads on the stringers. The floor beams, stringers, clip angles, and the reinforced concrete deck of one panel were included in the model. 3D beam elements were used to model the floor beams and stringers. Orthotropic plate elements were used to model the reinforced concrete deck. The properties of the orthotropic plate elements were determined by performing an analysis of the reinforced concrete deck. Discussion of this analysis is found in Section 4.2.1.

Beam elements with a length of 0.1 inches (2.5 mm) were used to model the boundary conditions created by the clip angles and floor beams. Since the boundary beam elements modeled the compliance of the floor beams, the longitudinal rotation of the floor beams was fixed. The area moment of inertia of the boundary beam elements was set so that the end rotation at the end of the stringer beam elements matched the rotation of the clip angle from the clip angle deflection analysis. When results became available from the 3D FEA model, the properties of the boundary beam elements were adjusted. Two boundary beam elements were developed from the results of the 3D FEA model. One modeled the connection details in the interior of the span, and the other modeled the connection details at the end of the span.

Models of an end panel and an interior panel were developed for the north- and southbound structures. One axle of the standard fatigue truck was used to load the models. The primary interest was in the distribution of loads on the stringers. It was observed that the properties of the boundary beam elements, the area moment of inertia of the stringers, and the longitudinal position of the axle did not play a significant role in the loading of the stringers. Individual loading on the stringers was found to be strongly dependent upon both the lateral position and the width of the load axle. This finding indicates that detailed knowledge about the position of the stringers in relationship to the lanes of traffic is important. It also demonstrates the necessity of having a fatigue truck that accurately represents the actual characteristics of trucks.

The stringer loads calculated from the global FEA model are presented in Section 4.3. The COSMOS command files can be found in Appendix B.

4.2.1 Reinforced Concrete Deck Analysis

A six-inch thick reinforced concrete deck transmits the traffic load to the stringers and floor beams. An analysis was performed to quantify the equivalent stiffness of the concrete deck. During construction, steel rebar was placed in longitudinal and transverse directions to provide tensile strength to the deck to support traffic loads. The position and amount of rebar in each direction was different. For this reason, it was necessary to quantify the reinforced concrete deck stiffness properties in each direction.

The orthotropic properties of the deck were calculated by following the procedure outlined in *Reinforced Concrete Design* (*Everard and Tanner 1966*). The properties in each direction were calculated independently. A beam of unit width, with the top portion of the beam associated with compression and the bottom portion associated with tension, was used to model the deck. The

reinforcing steel in the top region of the deck was placed in the compression portion of the model, and the steel in the bottom portion of the deck was placed in the tension portion. There was one exception to this approach: in the transverse direction, the deck was constructed so that sections of the rebar changed depth. The rebar was installed so that it was always in the portion of the deck that would be in tension. It was in the upper region of the deck over the stringers and in the lower region between the stringers. For this reason, the transverse rebar was placed in the tension portion of the model.

The assumption was made in the analysis that the concrete could only contribute strength in compression. This created a beam model that had concrete and steel on the compression side and steel alone on the tension side. Area moments of inertia per unit width were calculated for the transverse and longitudinal directions. The area moments of inertia were then used to find equivalent moduli of elasticity for a six-inch thick uniform deck. The resulting moduli of elasticity for the transverse and longitudinal directions were 1,300 ksi (8,964 MPa) and 546 ksi (3,765 MPa), respectively. See Appendix C for details of the analysis.

4.2.2 Model Validation

To quantify the live loading and to assist in validating the analysis, field testing was performed on the Winchester Bridge by ODOT. Five strain gauges were installed on the top of the bottom flanges at mid-span of three stringers and on two floor beams of one span of the northbound structure. The uniaxial, 350 ohm strain gauges had a gauge length of 0.25 inches (625 mm) and were used in a three wire quarter bridge configuration. Samples were taken at a rate of 60 Hz with a 30 Hz low pass filter. The sensitivity of the strain measurements was ± 10 microstrain.

Strain gauges were installed on the first and second floor beams of the first span. Two stringers from the first panel and one stringer from the second panel were fitted with strain gauges. Figure 4.4 shows the strain gauge location in relation to the stringers and floor beams.

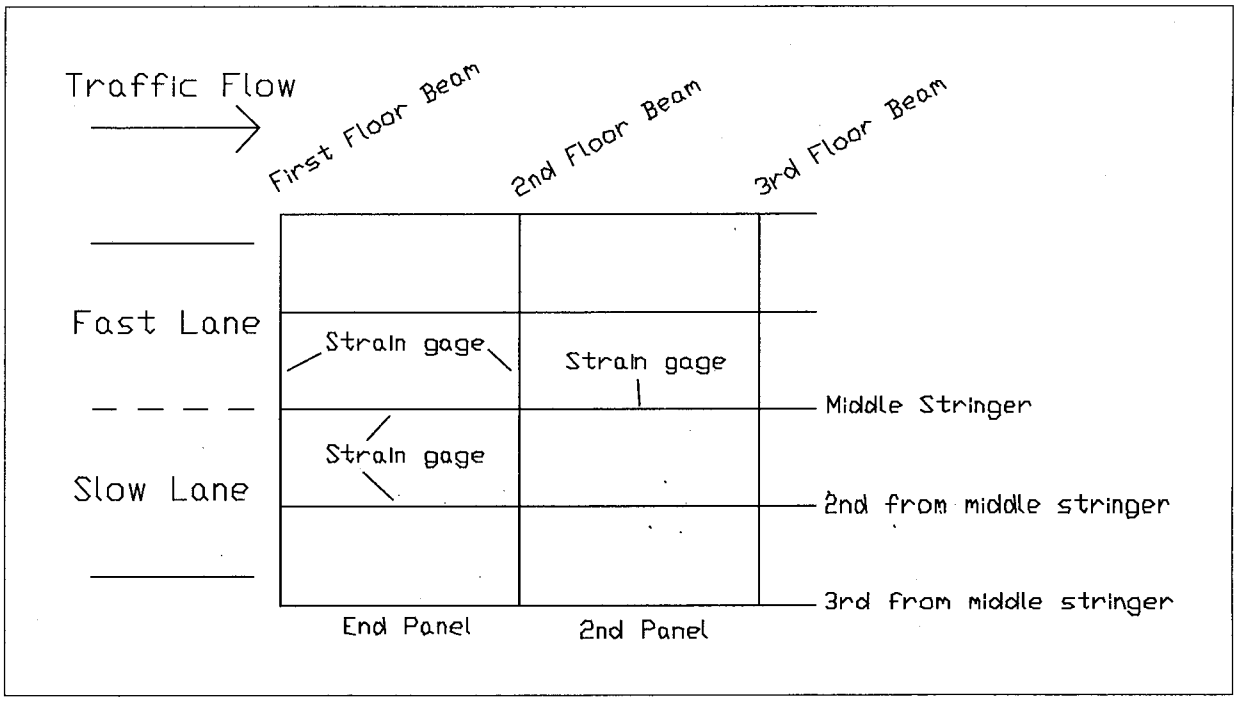

Figure 4.4: Location of strain gauges installed on three stringers and two floor beams on the northbound structure of the Winchester Bridge

Data were collected under normal traffic flow conditions with both lanes open and under a known truck weight with the slow lane closed. Figure 4.5 shows the comparison of the measured stress ranges in the stringers to those calculated from the global FEA model for the known truck weight. Figure 4.6 shows the comparison of the measured stress ranges in the stringers to those calculated from the global FEA model for random truck traffic. The cubed-root mean of the measured stress ranges for the random truck traffic are compared to the stress ranges calculated in the global FEA model loaded with the standard AASHTO fatigue truck. In Oregon the trucks comprising a random truck traffic sample are generally heavier than the AASHTO fatigue truck.

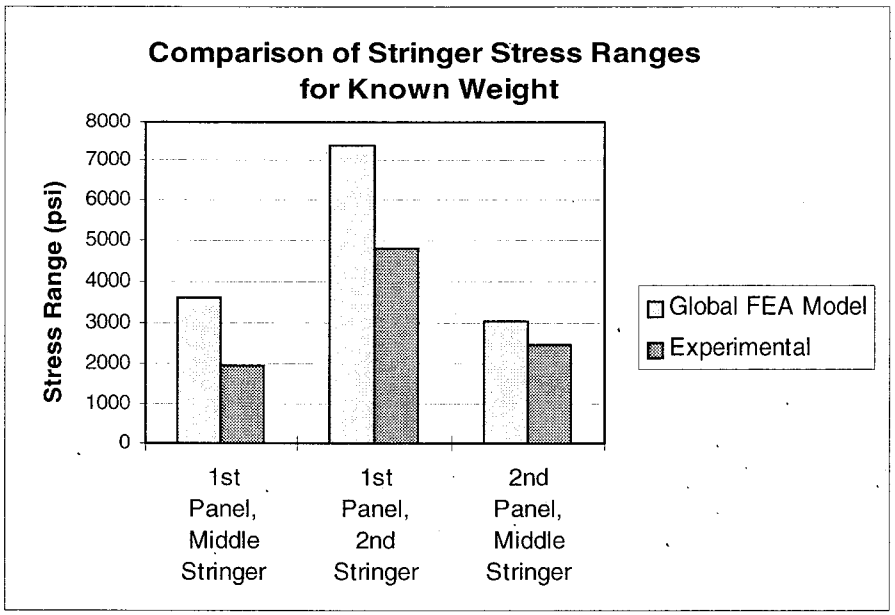

Figure 4.5: Stringer stress ranges from the global FEA model and those measured experimentally, loaded with a known truck weight

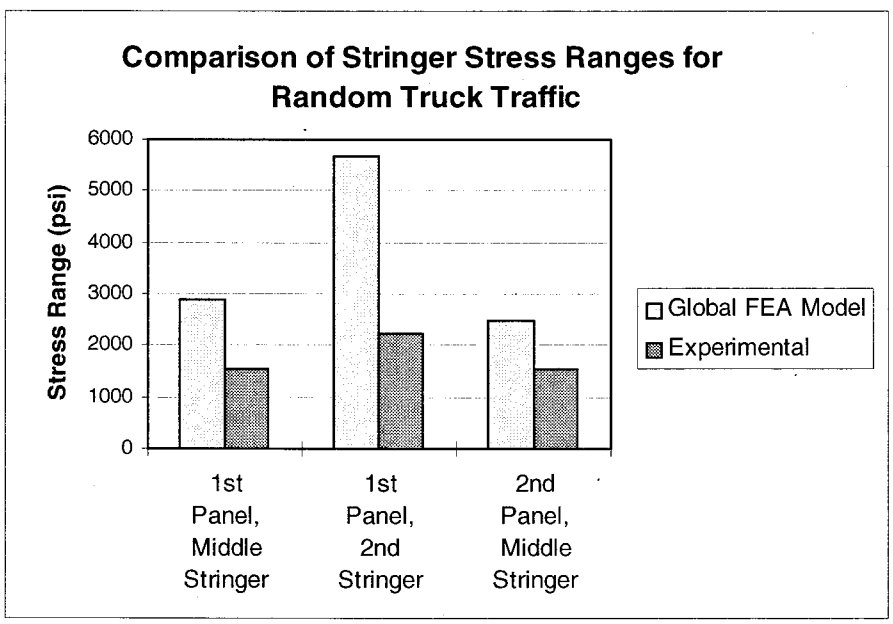

Figure 4.6: Stringer stress ranges from the global FEA model and those measured experimentally, under random traffic loading

The measured stresses are much lower than those calculated from the global FEA model. This occurs because the actual composite interaction between the deck and the stringers is not modeled in the global FEA model. If shear loads are transferred between the deck and the stringers, the neutral axis is shifted upward and the area moment of inertia is increased. This increases the section modulus for the stringer, resulting in a lower stress range.

The composite interaction between the deck and the stringers could be quantified if strain data were available for the top and bottom flanges. The ratio of strain ranges could be used to calculate the position of the neutral axis, and the known load and the strain range of the bottom flange could be used to calculate the section modulus. The effective area moment of inertia could be calculated from the new position of the neutral axis and the new section modulus.

Another possible reason for the difference in calculated and measured stress ranges is that the actual reinforced concrete deck is stiffer than calculated. Assuming that concrete only contributes compressive strength is a very conservative approach. A stiffer deck would increase the distribution of the axle load to other stringers.

4.3 RESULTS

A significant load was considered to be one greater than 3000 lb (1360 kg). Two stringers in each panel of the northbound structure were loaded significantly. They included the loads on the middle stringer and the second-from-middle stringer on the slow lane side. Figure 4.7 shows the stringer loads for the northbound structure.

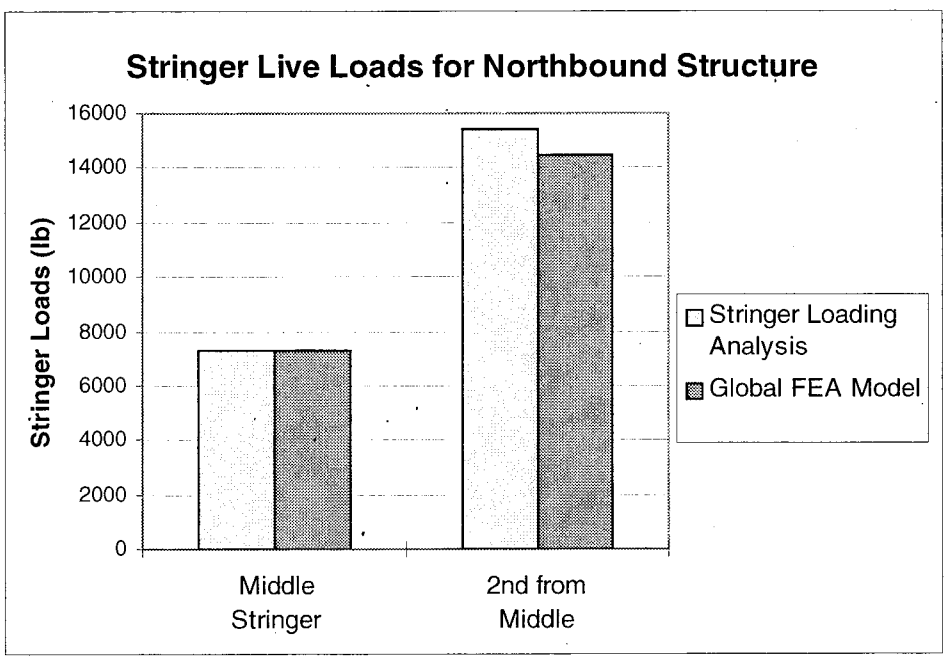

Figure 4.7: Stringer loads for the northbound structure for both the stringer loading analysis and the global FEA model

Three stringers in each panel of the southbound structure were also loaded significantly. They included the middle stringer, second-from-middle stringer, and the third-from-middle stringer on the slow lane side. Figure 4.8 shows the stringer loads for the southbound structure.

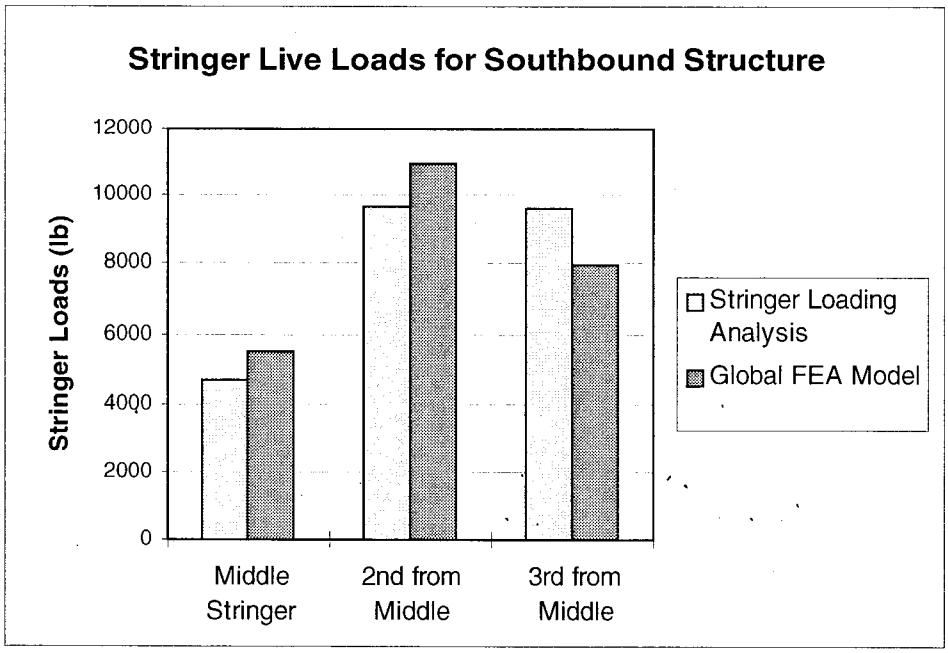

Figure 4.8: Stringer loads for the southbound structure for both the stringer loading analysis and the global FEA model

The results show that the two methods are in reasonable agreement. This is noteworthy because for the stringer loading analysis it was assumed that three stringers carry the entire axle load. These results suggest that this assumption is reasonable for a six-inch (150 mm) reinforced concrete deck.

Changes in the deck stiffness were investigated by increasing the deck thickness in the global FEA model. Figure 4.9 shows the loads on the second-from-middle stringer versus the deck thickness of both the north- and southbound structures.

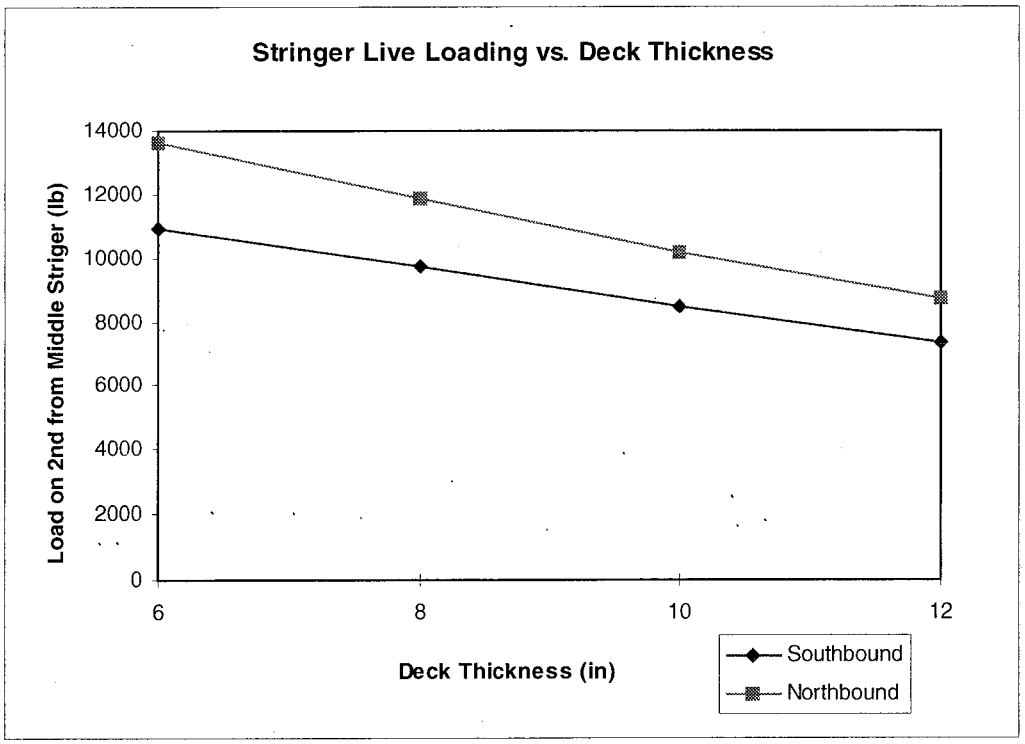

Figure 4.9: Load on the second from middle stringer vs. the deck thickness from the global FEA model

It can be observed that as the deck thickness is increased, the axle load is distributed to other stringers. This is an important finding since the reinforced concrete deck thickness varies on other structures. Information about the effect of deck thickness on the stringer can be used to estimate stringer loads in other bridge structures. The assumption that the effective moduli of elasticity on other bridge decks are the same as the moduli calculated for the Winchester Bridge, however, would have to be validated for any subsequent deck stiffness analysis.

5.0 DEFLECTION AND STRESS ANALYSIS

The clip angle creates a unique boundary condition for the stringer. The compliance of the clip angle connection is between that of an ideal fixed and an ideal pinned connection. When the stringer is loaded, there is a resulting end reaction moment (M_o) between the clip angle and stringer. The clip angle deflection (δ_m), the end stringer rotation (θ_{ST}), and the level of stress in the clip angle are dependent upon M_o. Since only live loading was considered, the maximum level of stress in the clip angle translates to a stress range. The three analysis techniques used to investigate these relationships are discussed in the following sections.

5.1 CLIP ANGLE DEFLECTION AND STRESS ANALYSIS

To determine the end moment (M_o) the stringer was modeled as a pinned beam with the moments (M_o) acting on the ends and the stringer load (P) acting in the middle. Figure 5.1 shows the model of the stringer.

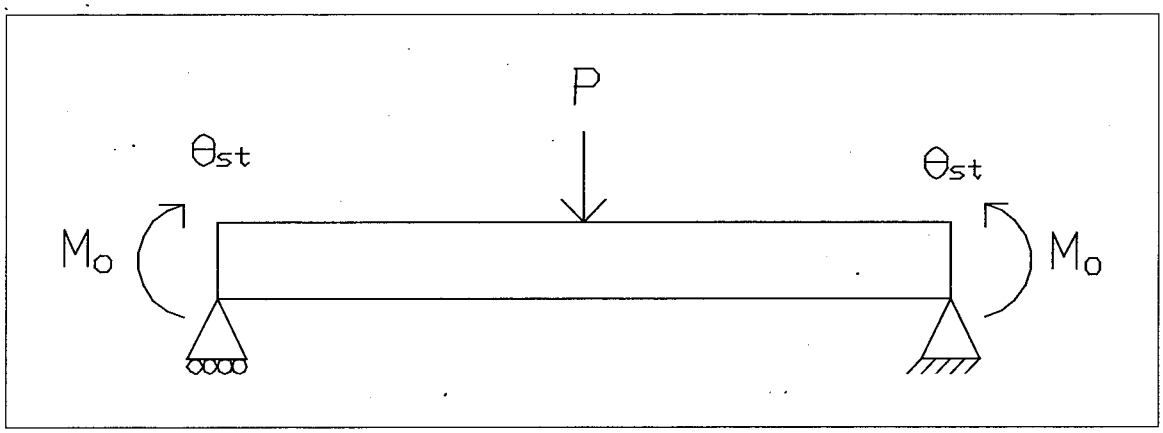

Figure 5.1: Stringer model, illustrating loading and boundary conditions

Using beam tables, the end rotation of the stringer (θ_{ST}) is written as:

$$\theta_{ST} = \frac{P \cdot L^2}{16 \cdot E \cdot I} - \frac{M_O \cdot L}{2 \cdot E \cdot I} \qquad \textbf{(5-1)}$$

where

L is the length of the stringer,

I is the area moment of inertia of the stringer, and

E is the Young's modulus of the stringer (*Gere and Timshenko 1990*).

An Euler beam analysis was performed to determine the deflection of the clip angle (δ_m) as a function of the end moment (M_o). To verify this relationship, the top of the floor beam leg of the clip angle was modeled as a cantilever beam with a force per unit length (F_R) and a moment per unit length (M_R) acting on the end. Figure 5.2 shows a diagram of the cantilever beam model of the clip angle.

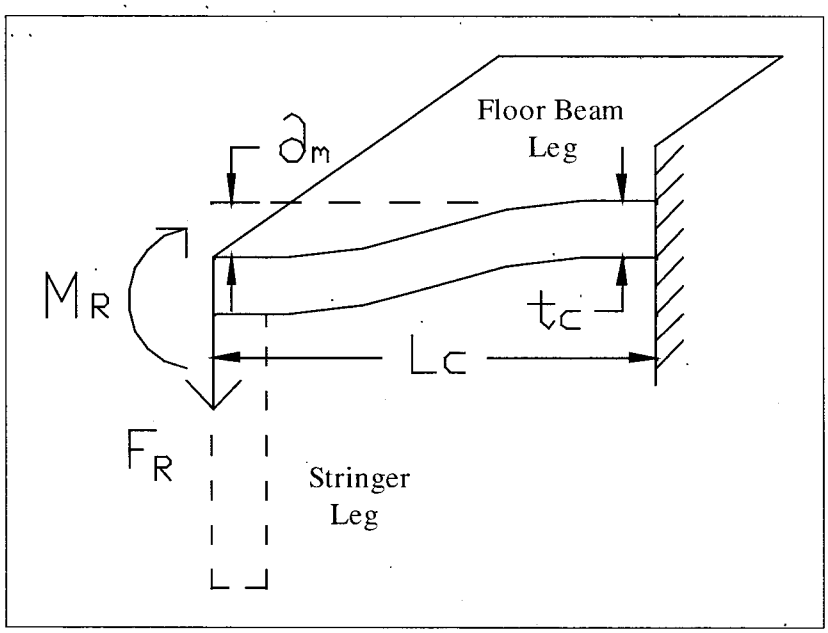

Figure 5.2: Top of the floor beam leg of the clip angle modeled as a cantilever beam

F_R is a result of the moment (M_o) and is calculated by assuming that the center of rotation of the clip angle is at the bottom. Figure 5.3 is a diagram showing how F_R is related to M_o. F_R is written as a function of M_o as:

$$F_R = \frac{3 \cdot M_o}{2 \cdot h^2} \tag{5-2}$$

where

h is the height of the clip angle.

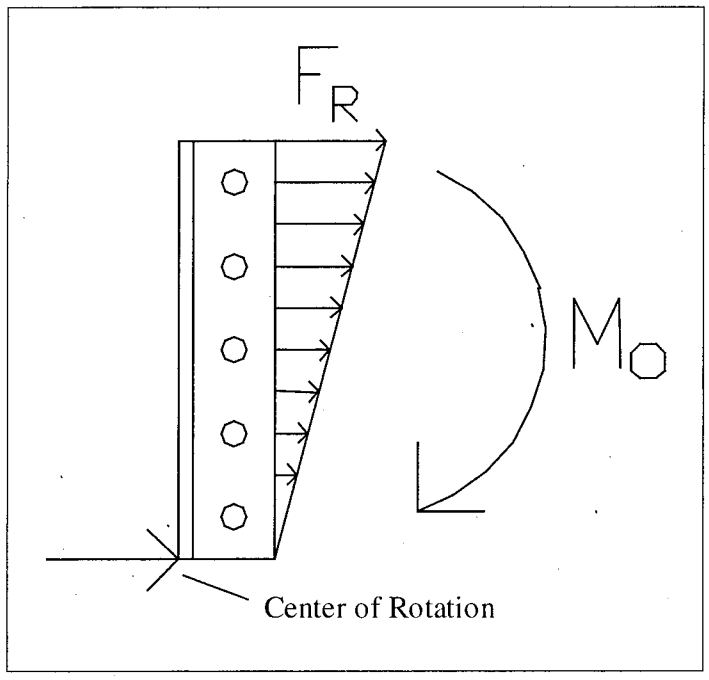

Figure 5.3: Diagram of clip angle showing the center of rotation and the relationship of F_R and M_o

The stringer leg of the clip angle restricts the rotation at the corner of the clip angle. For this reason, an assumption was made that rotation is zero for the clip angle at the end of the beam model. M_R is the moment at the corner of the clip angle restricting the rotation of the corner of the clip angle. By setting the end rotation equal to zero, M_R is a function of F_R, where:

$$M_R = \frac{F_R \cdot L_C}{2} \tag{5-3}$$

where

L_C is the length of the clip angle beam model.

The deflection (δ_m) of the clip angle was then found as a function of the end moment (M_o). The clip angle rotation is calculated (by small angle theorem) as the deflection divided by the height of the clip angle. The expression for the clip angle rotation is:

$$\theta_{cl} = \frac{\delta_m}{h} = C_R \cdot M_o \tag{5-4}$$

$$C_R = \frac{3 \cdot L_C^{\ 3}}{2 \cdot E \cdot t_C^{\ 3} \cdot h^3} \tag{5-5}$$

where

C_R is the clip angle rotation constant,

L_C is the length of the beam,

E is the Young's modulus,

t_C is the clip angle thickness, and

h is the height of the clip angle.

Due to physical constraints, the rotation of the clip angle and the end rotation of the stringer must be equal. The moment was found as a function of both stringer and clip angle parameters and is shown as:

$$M_o = \frac{\dfrac{P \cdot L^2}{16 \cdot E \cdot I}}{C_R + \dfrac{L}{2 \cdot E \cdot I}} \tag{5-6}$$

where

P is the load on the stringer,

L is the length of the stringer,

I is the area moment of inertia of the stringer,

E is the Young's modulus of the stringer, and

C_R is the clip angle rotation constant.

This equation is important because values of C_R, which are determined from the results of the 3D FEA model, can also be inserted into the equation above to calculate M_o. See Appendix D for details of the derivation.

The moment in the leg of the clip angle is highest at the corner of the clip angle where the stringer leg and floor beam leg of the clip angle come together. However, the maximum stress range is not located at the corner because the corner fillet increases the clip angle thickness. See

Appendix E for calculation details of the maximum stress in the clip angle. The clip angle deflections and stress ranges can be found in Section 5.4, Results.

5.2 2D FEA MODEL

A 2D FEA model of the top section of the clip angle was developed to determine the deflections and stress ranges in the clip angles. Plain stress plate elements of unit depth were used to build the model. Figure 5.4 shows the boundary conditions and loading of the 2D FEA model.

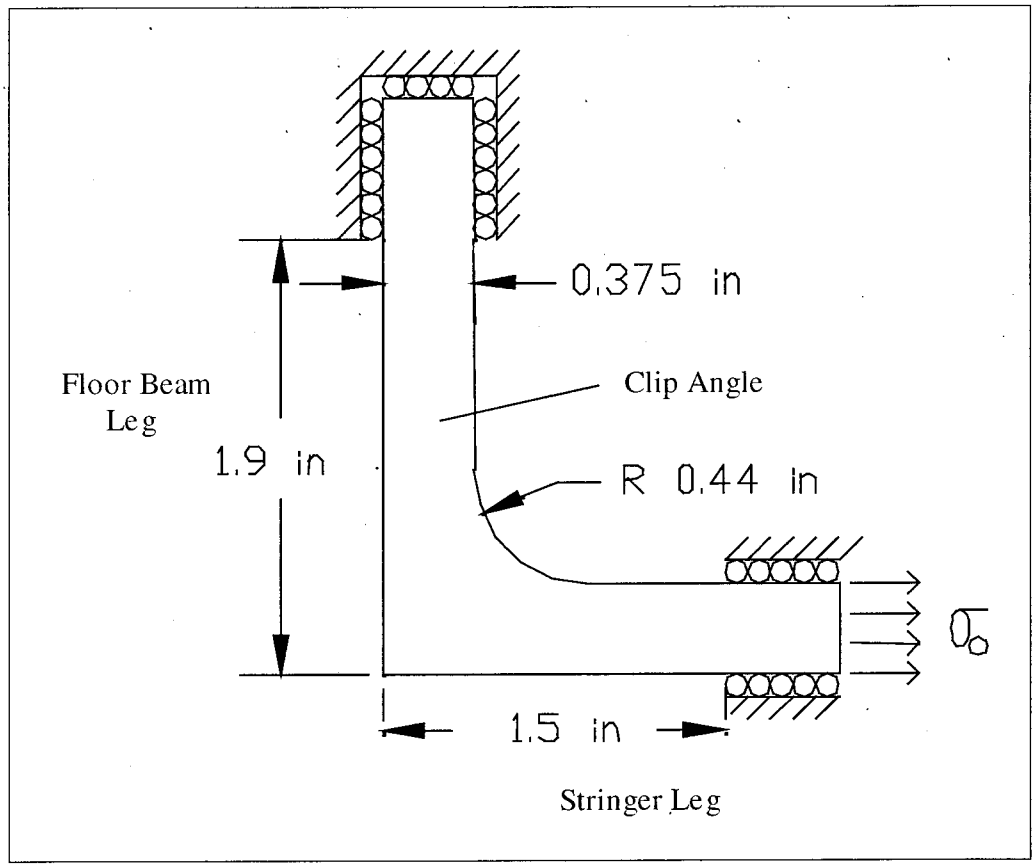

Figure 5.4: 2D FEA model of the top of the clip angle illustrating size dimensions, boundary conditions, and loading

Fixed boundary conditions were used to model the riveted connections of the clip angle to the floor beam and the stringer. An assumption was made that the riveted connections between the clip angle and the floor beam and stringer were at the top of the clip angle, when they were actually located 1.5 inches (38 mm) from the top. This simplification resulted in a reduction of compliance but was necessary because of the nature of the 2D model. A uniform pressure load, (σ_o), was applied to the stringer leg of the clip angle to model the axial loading at the top of the

clip angle from the stringer. The pressure load is a result of the moment (M_o) at the end of the stringer and is found by dividing the expression for the force per unit length (F_R), by the clip angle thickness. The expression for σ_o is:

$$\sigma_o = \frac{F_R}{t_C} = \frac{3 \cdot M_o}{2 \cdot t_C \cdot h^2} \tag{5-7}$$

where

t_C is the thickness of the clip angle,

h is the height of the clip angle, and

M_o is the moment transferred to the clip angle from the stringer.

Stress ranges and deflections for the different clip angles are presented in Section 5.4. The MAZE command files and further details of the analysis can be found in Appendix F.

5.3 3D FEA MODEL

A 3D FEA model of a clip angle, a stringer, and a section of floor beam was developed to accurately determine the deflection and the stress in the clip angle. The clip angle, stringer, and floor beam were meshed as separate parts with hexahedral brick elements. Symmetry planes were used to decrease the number of elements in the model. The model was divided into four quadrants by placing planes of symmetry, longitudinally down the center of the stringer and laterally at the midpoint of the stringer.

Slide-surfaces were used as interfaces between the three parts. The contact algorithms allow non-linearity, such as gaps and frictional sliding to be modeled.

The riveted connections between the stringer, clip angle, and floor beam were important parts of the model. The rivets used to connect the stringer and clip angle were meshed as part of the stringer. The rivets used to connect the floor beam and the clip angle were meshed as part of the floor beam. Slide surfaces were used between the rivets and the clip angle. A pre-load of 25 kip (11.3 metric tons) was applied to the rivets to approximate the as installed rivet pre-load.

The majority of steel deck truss span bridges under the responsibility of ODOT contain connection details that are made of 3.5 x 4 x 0.38 inch (90 x 100 x 9.5 mm) angles (as in the Winchester Bridge) and 3.5 x 4 x 0.50 inch (90 x 100 x 13 mm) angles. For this reason, both 0.38 and 0.50 inch (9.5 and 13 mm) thick clip angles were modeled and analyzed.

Several factors were investigated to determine their effect on the deflection and stress range of the clip angle. They are discussed in the following sections.

5.3.1 Element Density

Element density was the first factor investigated. Generally, the accuracy of a finite element model increases as the number of elements increases until the mesh is sufficiently fine. At this point, further mesh refinement does not yield a significant increase in accuracy. The analysis time is also increased as the number of elements is increased. The intent with element density is to use the minimum number of elements that still produce accurate results.

The effect of element density on the model was explored by changing the number of elements across the thickness of the clip angle. It was discovered that the deflections of the clip angle and the end rotation of the stringer did not depend significantly on the element density. The stress range did, however, depend on the density.

When the number of elements across the thickness of the 0.38 inch (9.5 mm) thick clip angle was increased from four to five, the maximum stress range increased by 8%. When the number of elements was increased from five to six, the maximum stress range only increased by 4%. It was concluded that, for the 0.38 inch (9.5 mm) thick clip angle, six elements across the thickness were adequate.

When the number of elements across the thickness of the 0.50 inch (13 mm) thick clip angle was increased from five to six, the maximum stress range increased by 17%. When the number of elements was increased from six to seven, the maximum stress range only increased by 5%. It was concluded that, for the 0.50 inch (13 mm) thick clip angle, seven elements across the thickness were adequate.

5.3.2 Boundary Conditions

The boundary conditions for the floor beam mesh made a significant difference in the deflection and stress of the clip angle. Floor beams at the end of the span with stringers connected to only one side have different boundary conditions than floor beams in the interior of the span with stringers connected to both sides. Two sets of boundary conditions were investigated for the floor beam mesh. They were the fixed rotation model and the fixed top flange model.

The interior floor beams were modeled using the fixed rotation model. In this model, the floor beam rotation is fixed throughout the length of the mesh. For the model, it was assumed that rotation of the interior floor beams was zero because their rotation was restricted by stringers attached to both sides.

The floor beams at the end of the span were modeled using the fixed top flange model. In this model, the ends of the floor beam and the top flange of the floor beam were fixed. The top flange of the floor beam was fixed to model the restriction that the reinforced concrete deck applied to the floor beam.

5.3.3 Rivet Pre-load and Friction

Rivet pre-load and friction were used to increase the accuracy of the riveted connection. The rivet pre-load is applied by lowering the temperature of the rivets, causing them to thermally

contract. This is done in a time step before the stringer is loaded. Friction was applied by changing the coefficient of friction from 0.0 to 0.5. The static and sliding coefficients of friction for mild steel on mild steel are 0.74 and 0.57 respectively. (*Marks 1996*).

When friction and rivet pre-load were applied to the model, the connection between the stringer and clip angle was changed. The rivet pre-load produced high normal forces at the interfaces between the stringer, clip angle, floor beam, and rivets. The frictional forces increased the stiffness of the connection between the stringer and the clip angle, reducing the end rotation of the stringer and increasing the flexural moment transmitted to the clip angle.

The pre-load and friction also changed the stress flow through the clip angle. When there was no pre-load and friction, the load from the rivet was forced to go around the rivet holes. When pre-load and friction were applied, the load was transmitted across the rivet hole by the frictional forces between the rivet, clip angle, and stringer. This resulted in a more localized stress concentration in the clip angle. The location of the stress concentrations will be discussed in Section 5.4.

5.3.4 Clip Angle Thickness

The clip angle thickness was another factor investigated. Models were created for 0.38 inch (9.5 mm) and 0.50 inch (13 mm) thick clip angles. For the same loading and floor beam boundary condition of fixed rotation, the deflection of the 0.50 inch (13 mm) clip angle was 28% lower than the 0.38 inch (9.5 mm) clip angle, and the maximum stress range decreased by 8%. The rotation of the end of the stringer with the 0.50 inch (13 mm) clip angle was about 12% lower than the 0.38 inch (9.5 mm) clip angle.

The stress ranges for the different clip angles are presented in Section 5.4. The stress ranges are from models that included friction and pre-load. A True Grid command file and additional results can be found in Appendix G.

5.4 RESULTS

Figures 5.5 and 5.6 are exaggerated deflection plots for interior panel clip angles from the 2D FEA model and 3D FEA model, respectively.

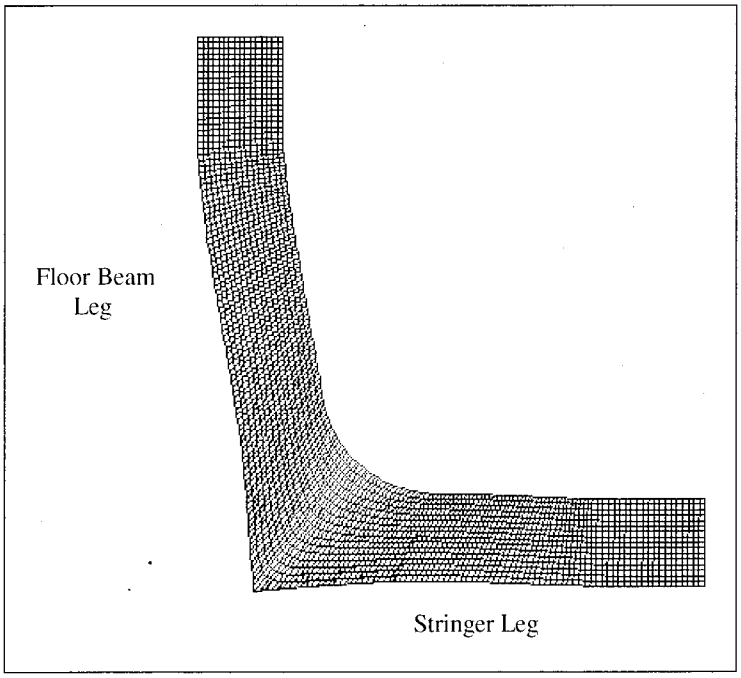

Figure 5.5: Exaggerated deflection plot from the 2D FEA model of an interior panel clip angle

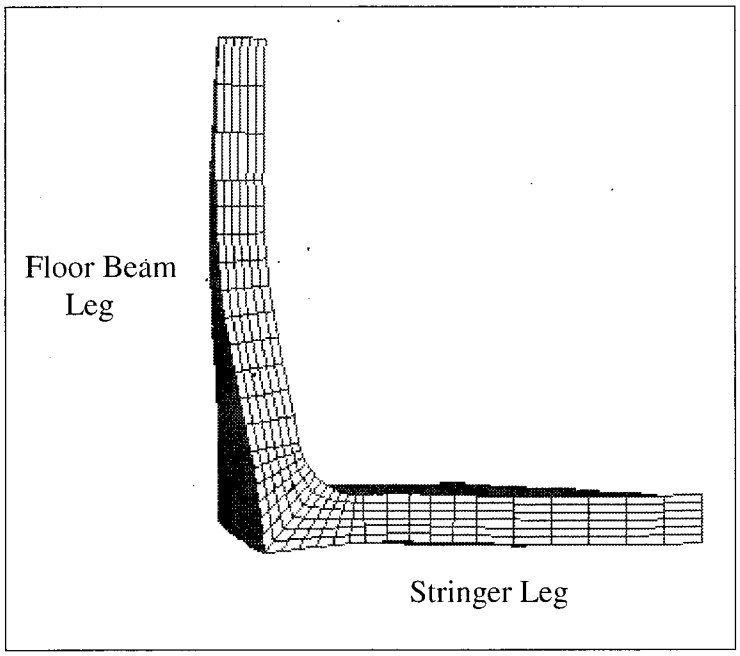

Figure 5.6: Exaggerated deflection plot from the 3D FEA model of an interior panel clip angle

The shape of the two plots appear very similar: they both show that there is rotation at the corner. This indicates that the assumption made in the clip angle deflection analysis, that the rotation of the corner of the clip angle is zero, is incorrect.

The results from the clip angle deflection analysis and the 2D FEA model represent clip angles located in the interior panels only. Table 5.1 shows the deflections calculated from each analysis method for the interior panel clip angles.

Table 5.1: Comparison of Interior Panel Clip Angle Deflections (in.) from Each Analysis Method

Analysis Method	Northbound		Southbound		
	Middle	Second	Middle	Second	Third
Clip Angle Deflection Analysis	0.0019	0.0037	0.0014	0.0029	0.0021
2D FEA Model	0.0039	0.0078	0.0031	0.0061	0.0044
3D FEA Model	0.0033	0.0066	0.0025	0.0050	0.0036

The clip angle deflection analysis predicts the lowest clip angle deflection. The reason that the clip angle deflections were so low, compared to the other two analyses, was because of the (incorrect) assumption of zero rotation at the clip angle corner. Both the 2D FEA and 3D FEA deflection plots show that the rotation was restricted but not zero.

The deflection predicted from the 3D FEA model was about 16% smaller than the deflection predicted from the 2D FEA model. This occurred because in the 3D FEA model, there was relative movement between the stringer and clip angle. In the 2D FEA model, a simplifying assumption was made that the rotation of the clip angle and rotation of the end of the stringer were the same. The relative movement adds to the compliance of the connection, reducing the flexural moment applied to the clip angle.

Figure 5.7 is a fringe plot of the maximum principle stress from the 2D FEA model. This plot is based on a 10 kip (4.5 metric tons) stringer load, and the fringe plot displays a range of stress values from 14,000 psi (96.5 Mpa) to 34,000 psi (234.4 Mpa).

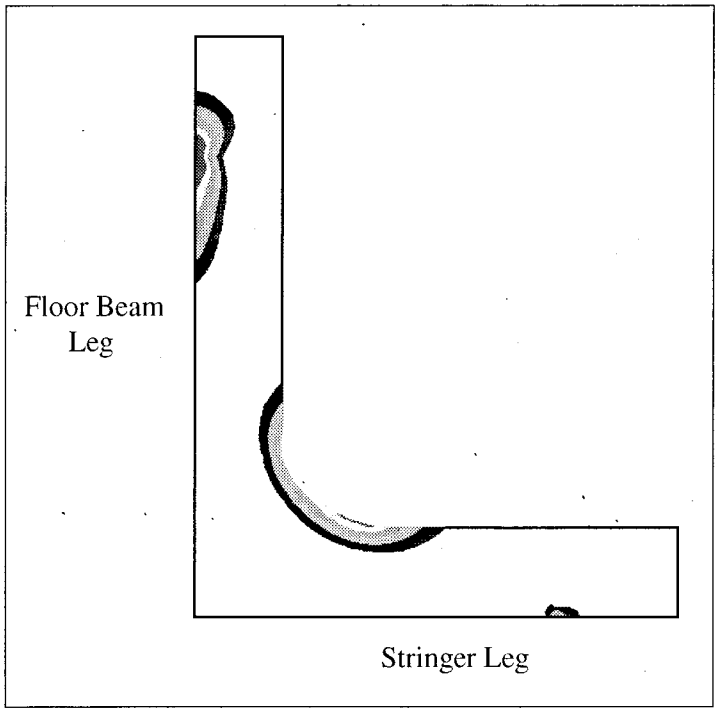

Figure 5.7: Fringe plot of the maximum principal stress for an interior panel clip angle from the 2D FEA model

There are two areas that achieve peak stress levels. The first is located at the base of the clip angle where it is attached to the floor beam. This peak stress is not relevant because the riveted connections are simplified at that location. The other peak stress area is located at the root of the fillet on the stringer leg.

The fixed rotation model of the floor beam is used to model the clip angles attached to interior floor beams. The fixed top flange model of the floor beam is used to model the clip angles attached to floor beams at the end of the span. Figure 5.8 is a fringe plot of the maximum principle stress from the 3D FEA model for clip angles in the interior panels (fixed rotation model). Figure 5.9 is a fringe plot of the maximum principle stress from the 3D FEA model for clip angles at the end of the span (fixed top flange model). In both cases, the stringer is loaded with 10 kip (4.5 metric tons), and the fringe plots display a range of stress values from 9,000 psi (62.1 Mpa) to 17,000 psi (117.2 Mpa).

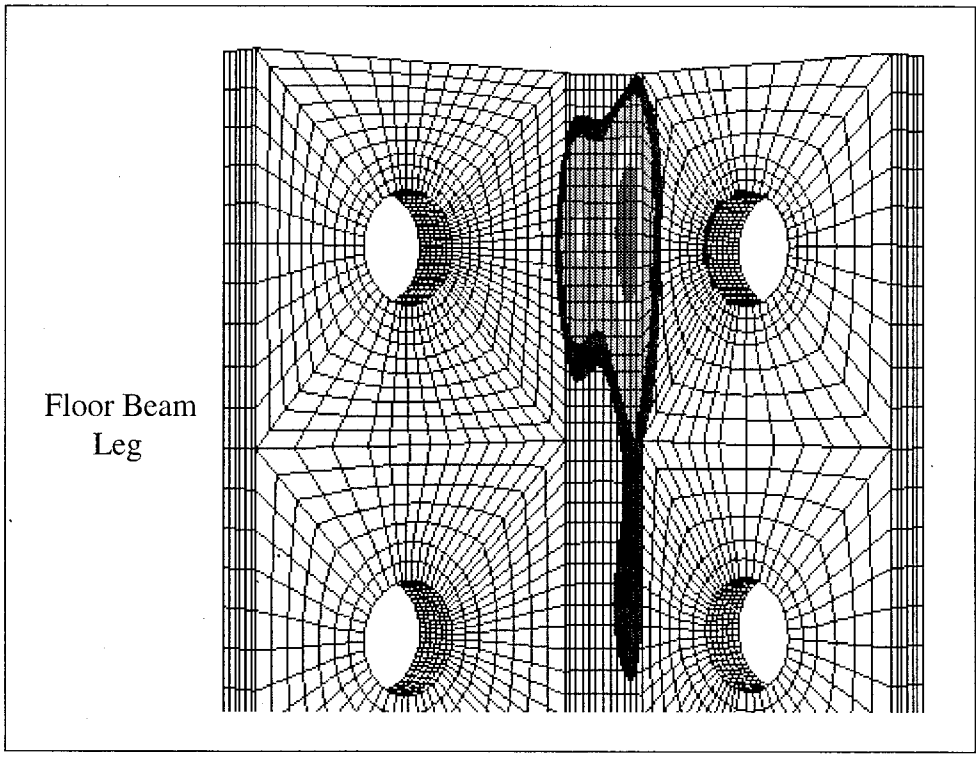

Figure 5.8: Fringe plot of the maximum principal stress from the 3D FEA model using the fixed rotation model of the floor beam.

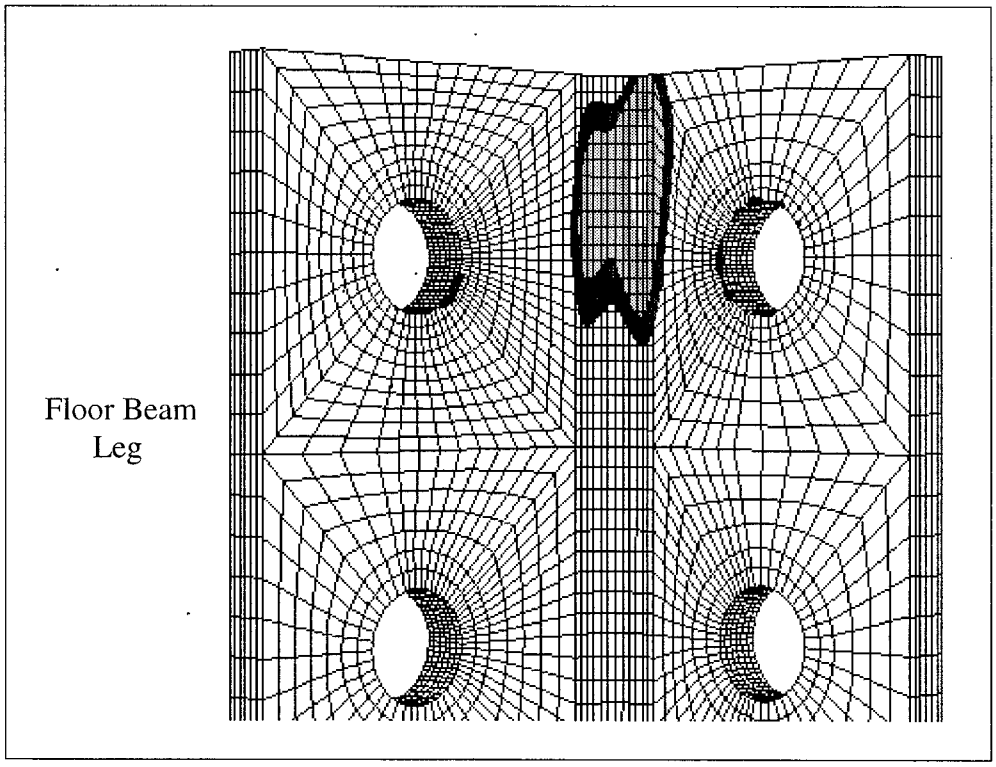

Figure 5.9: Fringe plot of the maximum principal stress from the 3D FEA model using the fixed top flange model of the floor beam

The fixed rotation model, illustrated in Figure 5.8, has a maximum stress range of 17,100 psi (118 Mpa). The fixed top flange model, illustrated in Figure 5.9, has a maximum stress range in the clip angle of 14,700 psi (101 Mpa), a value that is about 14% lower than the maximum in the fixed rotation model. The rotation of the end of the stringer in the fixed top flange model is calculated to be 0.00095 radians, whereas the rotation of the end of the stringer for the fixed rotation model is calculated to be 0.00065 radians. This is noteworthy in that the increase in stringer end rotation (and hence compliance) of 46% results in a decrease in stress range of only 14%.

The location of the maximum stress from both 3D FEA models match the location of the maximum stress found in the 2D FEA model. The maximum stress is located at the root of the fillet on the stringer side of the clip angle. There is a local area of high stress at the root of the fillet on the floor beam side. This is the same location of local area high stress calculated in the clip angle stress analysis. The stress at the root of the fillet on the floor beam side is composed only of bending stresses, while the stress at the root of the fillet on the stringer side is a combination of both axial and bending stresses.

Table 5.2 shows the stress ranges calculated from each analysis method for interior panel clip angles. The stress ranges calculated from the 3D FEA model were much smaller than those calculated from the 2D FEA model and the clip angle stress analysis. The relative movement between the stringer and the clip angle adds to the compliance of the connection, reducing the flexural moment applied to the clip angle. This results in a stress range reduction.

Table 5.2: Comparison of Interior Panel Clip Angle Maximum Stress Range (ksi) Results

Analysis Method	Northbound		Southbound		
	Middle	Second	Middle	Second	Third
Clip Angle Stress Analysis	21.6	42.9	16.6	33.1	24.0
2D FEA Model	22.8	45.2	17.8	35.5	25.7
3D FEA Model	12.5	24.8	10.1	20.1	14.6

As shown in Table 5.3, the longitudinal positions of the clip angles affect the magnitude of the moment loads transmitted to the clip angles and hence the stress range. When a stringer is loaded, the reaction moments at each end are dependent upon the boundary conditions at both ends. Clip angles attached to floor beams at the end of the span create a different boundary condition than clip angles attached to interior floor beams. Even though they represent the same boundary condition, clip angles in end panels attached to interior floor beams see higher loads than clip angles in interior panels, because the other end of the stringers have clip angles that create a more compliant boundary condition.

Table 5.3: Clip Angle Stress Range Results from the 3D FEA Model for Different Locations

Clip angle location	Northbound		Southbound		
	Middle	Second	Middle	Second	Third
Interior panel clip angles	12.5	24.8	10.1	20.1	14.6
End panel, interior floor beam clip angles	13.8	27.5	11.3	22.5	16.3
End panel, end floor beam clip angles	8.6	19.9	7.1	14.2	10.3

6.0 FATIGUE ANALYSIS

The stress ranges determined from the 3D FEA model using the stringer loads from the global FEA model were used in the fatigue analysis to estimate the fatigue life in load cycles of the different connection details. Two methods were used to calculate the life of the connection details. They were the stress-life approach and linear-elastic fracture mechanics approach. The strain-life approach was not used because the connection details are undergoing high cycle fatigue, and the strain-life approach is only appropriate for low cycle fatigue. An overview of the three analysis methods is presented in Section 3.3.

Part of the analysis was to convert the fatigue life in load cycles to remaining fatigue life in years. The following sections describe the two fatigue analysis methods and the calculation of remaining fatigue life. Results of the fatigue analysis are presented in Section 6.4.

6.1 STRESS-LIFE

The stress-life method is based on comparing an alternating stress amplitude to a stress versus life curve, an S-N diagram. The constant amplitude endurance limit needs to be calculated to construct the S-N diagram. The ideal endurance limit was taken as $0.5 \cdot S_{UT}$. The ultimate tensile strength was chosen as 58 ksi (400 MPa), the lowest expected ultimate tensile strength for low carbon ASTM A-36 steel. (*Marks 1996*) The endurance limit was then calculated by applying the following modifying factors (*Shigley and Mischke 1989*):

$$C_{SF} = 14.4 \cdot S_{UT}^{-0.718} = 0.78 \qquad \textbf{(6-1)}$$

Surface Finish - (hot rolled)

$$C_S = \left(\frac{t}{0.3}\right)^{-0.1133} = 0.94 \qquad \textbf{(6-2)}$$

Size - (thickness at fillet t = 0.5)

$$C_L = 0.96 \qquad \textbf{(6-3)}$$

Loading - (bending and axial)

$$C_T = 1 \tag{6-4}$$

Temperature - (normal)

$$S_e = C_{SF} \cdot C_S \cdot C_L \cdot C_T \cdot 0.504 \cdot S_{UT} = 20.7 \text{ ksi} \tag{6-5}$$

Endurance Limit

With the endurance limit established, the S-N diagram was constructed. The equation for the number of cycles to failure is:

$$N = 10^{-\frac{C}{b}} \cdot S^{\frac{1}{b}} \tag{6-6}$$

where

$$b = \frac{1}{3} \cdot \log\left(\frac{0.9 \cdot S_{UT}}{S_e}\right),$$

$$C = \log\left[\frac{(0.9 \cdot S_{UT})^2}{S_e}\right],$$

N is the number of cycles, and

S is the alternating stress amplitude.

Because of the wide range of truck sizes and weights, bridge loading is variable in amplitude. The stress range results from the 3D FEA model are the effective variable amplitude stress ranges because the loading on the model is based on the suggested standard fatigue truck. The effective stress range obtained from the 3D FEA model was converted to an equivalent stress amplitude, S_N, using the Goodman relationship. The constant amplitude S-N relationship was then used for a variable amplitude loading by eliminating the infinite life region. The fatigue life in load cycles was then converted to remaining life in years. The remaining life of each of the different clip angles is presented in Section 6.4. See Appendix H for details of the calculations.

6.2 LINEAR-ELASTIC FRACTURE MECHANICS (LEFM)

The first step in determining the fatigue crack growth rate is to calculate the alternating stress intensity factor. Equation (6-7) (*Fisher, et al. 1989*) was used to calculate the alternating stress intensity factor:

$$\Delta K = F_e \cdot F_s \cdot F_w \cdot \Delta\sigma \cdot \sqrt{\pi \cdot a} \tag{6-7}$$

where

a is half the crack length,

$\Delta\sigma$ is the alternating nominal stress,

F_e is a factor for crack shape,

F_s is a factor to account for a surface crack, and

F_w is a factor for a specimen with finite width (*Fisher, et al. 1989*).

An elliptical crack shape was assumed where a is half the length of the crack and c is half the width of the crack. The factor F_e is written as (*Barsom and Rolfe 1987*):

$$F_e = \sqrt{\frac{1}{\varphi(a)^2 + 0.5\frac{\Delta\sigma}{\sigma_{ys}}}} \tag{6-8}$$

$$\varphi(a) = \int_0^{\pi/2} \left(1 - \left(\frac{c^2 - a^2}{c^2}\right) sin(\theta i^2\right)^{\frac{1}{2}} \cdot d\theta \tag{6-9}$$

A surface crack was assumed since the maximum stress occurs at the surface. F_s equals 1.12 for surface cracks. For surface cracks, the length (a) is the measurement from the surface to the crack tip. It is often referred to as the crack length instead of one half crack length. Also, based on discussions with ODOT, a Mode I (tension) loading was assumed.

Since the thickness of the clip angle is small, a factor for finite width was necessary and is written as follows (*Barsom and Rolfe 1987*):

$$F_W = 1.0 + 1.2\left(\frac{a}{t} - 0.5\right) \tag{6-10}$$

where

t is the thickness at the location of peak stress, and

a is the crack length.

The next step was to solve the Paris equation for the number of cycles to failure. In order to solve the Paris equation, initial and final crack sizes were needed. The final crack size was set as the thickness of the clip angle at the point of maximum stress. Using this final crack size will result in a prediction of the number of cycles for the crack to propagate through the thickness of the clip angle. This condition for the final crack size is based on the field inspection procedures used by ODOT and assumes that the clip angle will be replaced when a visible crack is observed. A maximum possible crack size (one that would produce clip angle failure) was not used, as this crack size would exceed ODOT's standard for end-of-service life.

The initial crack size is both more critical and more difficult to determine. The sizes of flaws in the clip angles vary randomly. Therefore, obtaining an accurate initial crack size is extremely difficult. For the purposes of this study, an initial crack size of 0.01 inches (0.25 mm) was used in the model. The fatigue model ignores the crack initiation phase, a phase that can account for a significant portion of fatigue life. The fatigue life, in load cycles, was then converted to remaining life in years. The remaining life of the different clip angles is presented in Section 6.4. See Appendix I for details of the calculations.

6.3 REMAINING FATIGUE LIFE

This section discusses how the remaining fatigue life in years for the clip angles was calculated from the fatigue life in load cycles. The first step in calculating the remaining fatigue life was to ascertain the traffic over the Winchester Bridge. The 1994 average daily traffic (ADT) and the traffic growth rate from 1984 and 1994 for the Winchester Bridge was obtained from the 1994 Traffic Volume Tables (*Oregon Department of Transportation 1995*). The ADT was determined using the linear function:

$$ADT(Y) = G + g \cdot Y \qquad \textbf{(6-11)}$$

where

G is the predicted ADT for 1997,

g is the growth rate, and

Y is the years starting at 1997.

The percent truck traffic of the traffic was found in the 1994 Traffic Volume Tables. Average daily truck traffic (ADTT) for the slow lane of each north and southbound structure was determined using:

$$ADTT(Y) = \frac{ADT(Y)}{2} \cdot F_T \cdot F_L \qquad \textbf{(6-12)}$$

where

F_T is the percent truck traffic found in the 1994 Traffic Volume Tables, and

F_L is the percent trucks in slow lane obtained from the NCHRP Report 299 (*Moses, et al. 1987*).

The ADT was divided by two to determine the average daily traffic for each individual structure.

To determine the number of load cycles to failure, the following relationship was used:

$$N_L = D \cdot C_L \int_{-A}^{L} ADTT(Y) \cdot dY \qquad \textbf{(6-13)}$$

where

N_L is the number of load cycles to failure,

D is the number of days in a year,

C_L is the load cycles per truck,

L is the remaining life of the detail, and

A is the current age of the structure.

The remaining life was found by integrating and solving for L.

6.4 RESULTS

Table 6.1 shows the remaining life in years of the different clip angles calculated using the stress-life approach. Table 6.2 shows the estimated remaining life in years for different clip angles calculated using LEFM. When the remaining fatigue life is a negative number, it means that the fatigue analysis predicts that the clip angles should have already failed.

Table 6.1: Estimated Remaining Life (Years) of the Different Clip Angles - Stress-Life Fatigue Analysis

Clip angle location	Northbound		Southbound		
	Middle	Second	Middle	Second	Third
Interior panel clip angles	182	-40	522	-20	68
End panel, interior floor beam clip angles	100	-42	308	-28	22
End panel, end floor beam clip angles	1056	-24	2340	83	477

Table 6.2: Estimated Remaining Life (Years) of the Different Clip Angles - Linear-Elastic Fracture Mechanics

Clip angle location	Northbound		Southbound		
	Middle	Second	Middle	Second	Third
Interior panel clip angles	9	-31	35	-18	1
End panel, interior floor beam clip angles	0	-34	22	-22	-8
End panel, end floor beam clip angles	57	-23	96	1	33

The remaining life values calculated for many of the clip angles are very low. The fact that both models predict that both structures should have experienced extensive fatigue damage many years ago indicates that the predicted stress ranges are probably too high. There are two explanations for why the stress ranges are high:

1) The model of the reinforced concrete deck may not have been stiff enough. If the deck were stiffer, the loads would be distributed more evenly to other stringers.

2) An effective area moment of inertia may need to be calculated to compensate for the composite interaction between the deck and the stringers. From Equation 5-6 it can be seen that when the area moment of inertia of the stringers increases, the flexural moments seen by the clip angles decrease.

The remaining life of the clip angles at the end of the span is predicted to be much higher than that of interior clip angles. This finding is unexpected, because for the southbound structure, fatigue cracks were only found in clip angles at the end of the spans. One possible explanation is that the added compliance of the connection details at the end of the span increases the tendency for them to vibrate, thus increasing the number of effective load cycles per truck. This vibration would have the effect of reducing the fatigue life of those connection details. The effect of vibration on the fatigue life of the connection details was beyond the scope of the project and was not investigated.

7.0 IDENTIFICATION METHODOLOGY

There are many bridge structures under the responsibility of ODOT, which are very similar to the Winchester Bridge. In this study a method was developed to quickly identify whether or not the structure contained problem details. The effects of several parameters on the stress range in the clip angles were investigated. The parameters included the reinforced concrete deck thickness, stringer spacing, stringer length, stringer area moment of inertia, and the thickness of the clip angle. Equations were developed that calculated the stress range of the clip angles that experienced the highest load. A high resulting stress range would indicate that the bridge contained problem details. A decision could then be made to determine if further analysis were necessary to ascertain which details had problems.

The effect of the reinforced concrete deck thickness on the stringer loading was investigated using the global FEA models of both the north- and southbound structures. When the deck thickness is six inches, the entire axle load is distributed among three stringers. As the deck thickness is increased, the axle load is distributed to other stringers and the floor beams. The reduction of load on the stringer with the maximum load is approximately linear and is about the same for both the southbound structure (63-inch (1.6 m) spacing) and the northbound structure (84-inch (2.1 m) spacing). Figure 4.9 in Section 4.3 shows the loads on the second-from-middle stringer versus the deck thickness of both the north- and southbound structures. The effect of the deck thickness was accounted for by multiplying the maximum stringer load by a linear expression dependent only on the deck thickness.

The effect of the stringer spacing on the load of the stringers was investigated using the results from the stringer loading analysis. The stringer loading analysis was used because it did not include the effects of the deck thickness, and the stringer spacing was easy to change. The load on the stringers depends on the lateral position of the axle load of the fatigue truck. Since lateral position may be unknown and the maximum stringer loads are desired, the worst case lateral position was found for each stringer spacing investigated. Figure 7.1 shows the load on the second-from-middle stringer versus the stringer spacing.

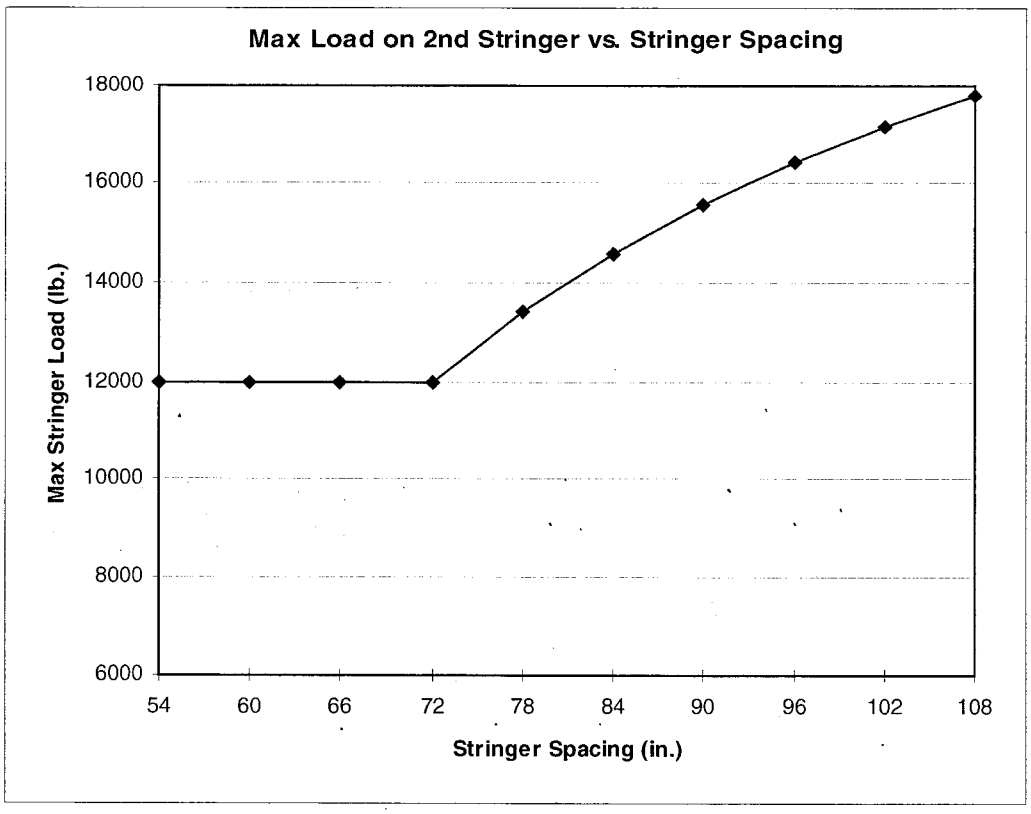

Figure 7.1: Load on the second-from-middle stringer vs. the stringer spacing

For a stringer spacing greater than the fatigue truck axle width (72 inches (1.8 m)), the relationship between the maximum load and the stringer spacing is approximately linear. This maximum load occurs when the fatigue truck axle is centered over a stringer. For stringer spacing less than the fatigue truck axle width, the maximum stringer load is constant and occurs with one wheel of the axle positioned directly over the stringer. The maximum stringer load is determined by using an expression that has asymptotes of the lines in each regime. The expression for the maximum stringer load, including the effects of both the reinforced concrete deck thickness and the stringer spacing, is shown as:

$$P = 12000\left(1 - \frac{t - 5.9}{17}\right) \qquad 0 < S < 72 \qquad \textbf{(7-1)}$$

$$P = 172S\left(1 - \frac{t - 5.9}{17}\right) \qquad 72 < S < 108 \qquad \textbf{(7-2)}$$

where

P is the maximum stringer load,

S is the width between the stringers, and

t is the thickness of the deck.

Equation 5-6, developed in the clip angle deflection analysis, was used to calculate the end moment applied to the clip angle, based on the stringer load, stringer length, stringer area moment of inertia, and the thickness of the clip angle. It is shown as:

$$M_o = \frac{\dfrac{P \cdot L^2}{16 \cdot E \cdot I}}{C_R + \dfrac{L}{2 \cdot E \cdot I}} \tag{7-2}$$

where

M_o is the end moment applied to the clip angle,

P is the maximum stringer load,

L is the length of the stringer,

I is the area moment of inertia of the stringer,

E is Young's modulus of steel, and

C_R is the clip angle rotation constant (dependent on the thickness of the clip angle).

The stress range is calculated by multiplying end moment (M_o) by the clip angle stress constant (C_S) (dependent on the thickness of the clip angle):

$$\sigma = C_S \cdot M_O \tag{7-3}$$

The clip angle constants, for both rotation and stress, relate the end rotation and stress in the clip angle to the end moment, and they are dependent on the size and shape of the clip angle. Constants are based on the results from the 3D FEA model and are available for both 3.5 x 4 x 0.38 inch (90 x 100 x 9.5 mm) and 3.5 x 4 x 0.50 inch (90 x 100 x 13 mm) clip angles.

This identification methodology was developed for interior panel connection details. The recommended method of investigating a bridge is to first use the stringer area moment of inertia to calculate a stress range. If the stress range is high, a more detailed investigation should be performed using the effective area moment of inertia of the deck and stringers. The effective area moment of inertia can be determined by using strain data taken from the top and bottom flanges of several stringers loaded with a known weight. The ratio of strain between the top and bottom flanges of the stringers can be used to calculate the change in the position of the neutral axis. The known load and the strain range of the bottom flange of the stringers can be used to calculate the effective section modulus. The actual position of the neutral axis and the effective section modulus can be used to calculate the effective area moment of inertia of the stringer and

deck. Using the effective area moment of inertia will give more accurate estimates for the stress range. Details of the procedure can be found in Appendix J.

8.0 RETROFIT STRATEGIES

The majority of steel deck truss span bridges under the responsibility of ODOT contain connection details that are made of 3.5 x 4 x 0.38 inch (90 x 100 x 9.5 mm) clip angles (such as on the Winchester Bridge) or 3.5 x 4 x 0.50 inch (90 x 100 x 13 mm) clip angles. Figure 2.3 in Chapter 2 illustrates the 3.5 x 4 x 0.38 inch (90 x 100 x 9.5 mm) clip angle. The analysis of both of these clip angles is discussed in Chapter 5.

Five retrofit strategies were investigated to determine their effectiveness in reducing the stress range developed in the connection details. They included the following:

1) Replacing clip angles with 4 x 6 x 0.38 inch (100 x 150 x 9.5 mm) angles.

2) Replacing clip angles with 4 x 6 x 0.50 inch (100 x 150 x 13 mm) angles.

3) Removing the top row of rivets from the clip angles.

4) Removing the top two rows of rivets from the clip angles.

5) Geometric stiffening of the stringer.

All of the retrofit strategies were modeled using the fixed rotation model of the floor beam, a 10 kip (4.5 metric tons) load, and a rivet pre-load of 25 kips (11.3 metric tons). The maximum stress ranges of each retrofit strategy was compared to the maximum stress range from 3.5 x 4 x 0.38 inch (90 x 100 x 9.5 mm) clip angle modeled under the same loading and boundary conditions.

The first two retrofit strategies differ only in the thickness of the angle. Figure 8.1 shows the angle used in strategy #1. The new clip angles are attached to the stringers and floor beams with bolts instead of rivets. For the clip angle - to - stringer connection, the same holes in the stringer are used for the bolts. For the clip angle - to - floor beam connection, the location of the holes changes. Four bolts are used instead of five, so that the new holes in the floor beam are located away from the old holes. This is done to retain the structural integrity of the floor beam. Retrofit strategy #2 was used to replace damaged clip angles on the Winchester Bridge in 1994.

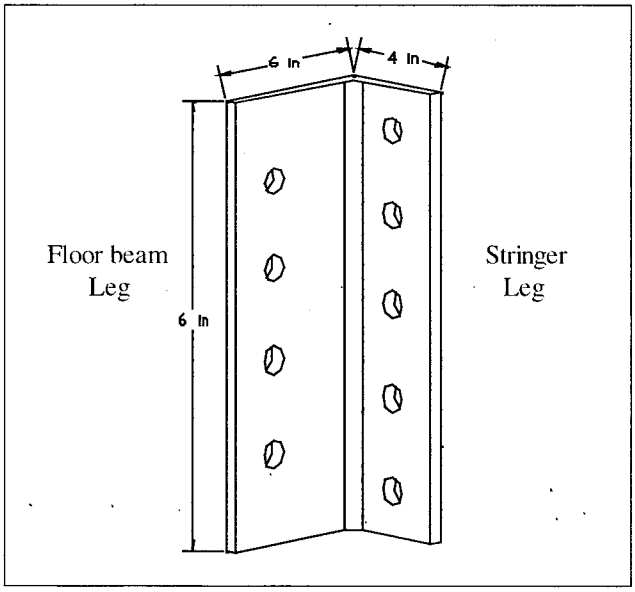

Figure 8.1: Retrofit strategy #2 used to replace damaged clip angles on the Winchester Bridge in 1994

Retrofit strategies #1 and #2 were designed to increase the compliance of the clip angle. The longer floor beam leg increases the compliance of the connection, reducing the flexural moment transmitted to the clip angle. The resulting deflection from strategy #1 is an increase of 10% over that of the existing clip angle. Using strategy #2 results in a deflection increase of 5%. The stress range for strategy #1 is 73% of the stress range for the existing clip angle. The stress range for strategy #2 decreases to 60%. The results show that increasing the compliance does reduce the stress range in the clip angle. It is also apparent that increasing the thickness of the clip angle reduces the stress range in the clip angle.

Retrofit strategies #3 and #4 involve removing rivets from the existing clip angles. In strategy #3 the top row of rivets that attach the clip angle to the floor beam and stringer is removed. In strategy #4 the top two rows of rivets that attach the clip angle to the floor beam and stringer are removed. Strategy #4 also includes installing a bracket under the stringer to relieve the shear load on the remaining three rows of rivets. The bracket was located in the model so that it supported the stringer directly under the location of the stringer rivets.

Retrofit strategies #3 and 4 are also designed to increase the compliance of the connection. They are different from strategies #1 and #2, in that compliance is added to the connection between the clip angle and stringer, not in the clip angles themselves. The stress range for strategy #3 is 68% of the stress range for the existing clip angle. The stress range for strategy 4 is 30% of the original stress range. The bracket used to transmit shear loads did not significantly affect the stress range in the clip angle. The increased compliance of the connection afforded by strategies #3 and #4 may have adverse effects on other structural members, in particular the reinforced concrete deck. These effects were not quantified.

In retrofit strategy #5 geometric stiffening is achieved by attaching one-inch (25 mm) diameter, high strength, wire rope to the bottom of the stringer. The wire rope is fastened to the bottom flange at each end of the stringer. At mid-span the wire rope is attached to a strut that pushes the rope 12 inches (300 mm) below the bottom of the stringer. Figure 8.2 shows a diagram of retrofit strategy #5.

The wire rope is pre-loaded to a stress of 6 ksi (41 Mpa). When the wire rope is pre-loaded, a force is applied to the stringer that opposes the live loading on the stringer. The wire and stringer also form a truss structure that increases the stiffness of the assembly. As the stringer is loaded, the wire rope resists the deflection of the stringer. The tension of the wire rope will pull on the bottom flange of the stringer resisting the end rotation. Also, as the tension increases, a force at the strut will be applied upward to the stringer that will oppose the load on the stringer. The stress range for strategy #5, with a one-inch diameter wire rope pre-loaded at 6 ksi (41 Mpa), is 76% the stress range of the original clip angle.

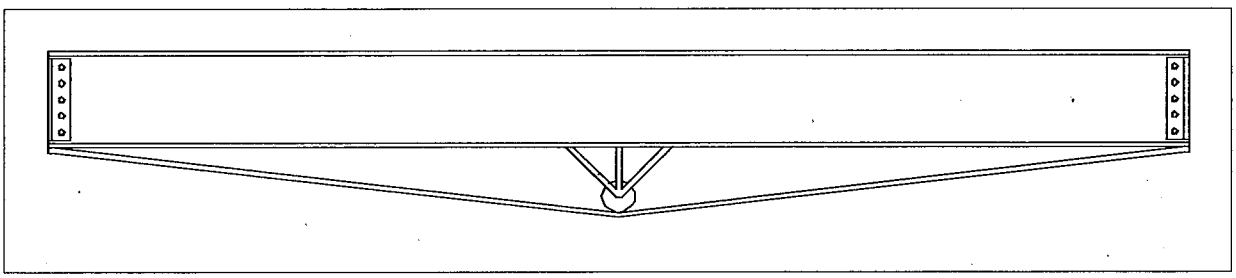

Figure 8.2: Diagram of the retrofit strategy #5, geometric stiffening

Table 8.1 shows a summary of the retrofit strategies and their relative effectiveness.

Table 8.1: Effectiveness of the Five Retrofit Strategies Investigated

Retrofit strategy	$\frac{\sigma\,(\text{retrofit})}{\sigma\,(3/8\text{ in. clip angle})}$
1) 4 x 6 x 0.38 inch angle	0.73
2) 4 x 6 x 0.50 inch angle	0.60
3) Removing top row of rivets	0.68
4) Removing top two rows of rivets	0.30
5) Geometric stiffening	0.76

9.0 SUMMARY, CONCLUSIONS AND FUTURE WORK

The Winchester Bridge is a typical steel deck truss bridge under the responsibility of ODOT, which contains connection details that are prone to fatigue. The primary function of the clip angles is to transmit end shear from the stringers to the floor beams. Since the clip angles are riveted to the stringers and floor beams, they are subjected to a flexural moment caused by the deflection of the stringer under live truck loads.

Even though strain data taken from the bridge indicates that the remaining fatigue life estimates are very conservative, the analysis performed for this report indicates that the connection details may be prone to fatigue damage. The conservatism of the analysis is believed to be a result of two factors:

1) underestimating the composite action of the deck and truss structures; and

2) conservative assumptions for initial and final crack sizes as used in the fatigue analysis.

We recommend additional field validation work to quantify the amount of composite action and hence the effective area moment of inertia and neutral axis location. These quantities could then be used to improve the accuracy of the stress and fatigue analyses. This additional validation work would include experimentally quantifying strain in the top and bottom flanges of the stringers and floor beams, for end and interior panels. The 3-D FEA analysis should then be repeated, adjusting the amount of composite action between the deck and the truss to obtain agreement with the field work.

The analysis indicates that the clip angles attached to the interior floor beams should experience the highest maximum stress ranges and hence exhibit the shortest fatigue lives. Actual experience with the bridge shows that the clip angles attached to the exterior floor beams were the most fatigue prone. The cause of this discrepancy remains to be determined.

The 3D stress analysis shows the area of maximum principle is fairly localized. The compliance added by a crack growing beyond this local area might result in lowered stress ranges and crack self-arrest. We recommend further analysis of this phenomenon with an FEA code that will handle the singularity associated with a fatigue crack. In addition, the fatigue crack growth model can be made more accurate by including the crack initiation phase.

A low cost field identification methodology was developed to determine whether other steel deck truss bridges contain problem details. The effects of parameters for the reinforced concrete deck thickness, stringer spacing, stringer length, effective stringer area moment of inertia, and thickness of the clip angle have been quantified. Equations were developed to quickly and easily estimate the stresses in the clip angles under the highest loads. The recommended method of investigating a bridge is to first use the stringer moment of inertia. If the stress range is high, a more detailed investigation should be performed using the effective area moment of inertia of the

deck and stringers. The effective area moment of inertia would be obtained experimentally. The accuracy of the equations used in this field identification methodology needs to be validated with experimental data.

Five retrofit strategies, suggested by the ODOT Technical Advisory Committee, were investigated to determine their effectiveness at reducing the stress range in the clip angles. As a result of the analysis, the most effective method is to remove the top two rows of rivets from the clip angles (retrofit strategy #4). Furthermore, this strategy would involve less installation work than replacing the clip angles (as in strategies #1 and #2 above), and would require less design work than geometric stiffening of the stringer (strategy #5). Removing only the top row of rivets (strategy #3) would be easier to implement than strategy #4 but it is not as effective at reducing the stress range as removing the top two rows of rivets. Removing rivets (as in strategies #3 and #4), however, will increase the shear loading on the remaining rivets unless additional details are added.

10.0 REFERENCES

Bannantine, J. A., Comer, J. J., and Handrock, J. L., *Fundamentals of Metal Fatigue Analysis.* Prentice-Hall, Inc., Englewood Cliffs, New Jersey. 1990.

Barsom, J. M., and Rolfe, S. T., *Fracture & Fatigue Controls in Structures.* Second Edition, Prentice-Hall, Inc., Englewood Cliffs, New Jersey. 1987

Cao, L., Allen, J. H., Shing, P. B., and Woodham, D., "Behavior of RC Bridge Decks with Flexible Girders," *Journal of Structural Engineering.* American Society of Civil Engineers, New York, New York. 1996

Christon, M. A., and Dovey, D., *INGRID User's Manual.* Lawrence Livermore National Laboratory, Livermore, California. 1992

COSMOS/M User's Guide, Volume 1, Version 1.70, Structural Research and Analysis Corporation, Santa Monica, California. 1993

Engelmann, B., *NIKE2D User's Manual.* Lawrence Livermore National Laboratory, Livermore, California. 1991

Everard, N. J., and Tanner, J. L., *Reinforced Concrete and Design.* McGraw-Hill Inc., New York, New York. 1966

Fisher, J. W., Mertz, D. R., and Zhong, A., "Steel Bridge Members Under Variable Amplitude Long Life Fatigue Loading." *NCHRP Report 267*, p. 22, Transportation Research Board, Washington, DC. 1983

Fisher, J. W., Yen, B. T., and Wang, D., "Fatigue of Bridge Structure - A Commentary and Guide For Design, Evaluation and Investigation of Cracking." *ATLSS Report No. 89-02*, Lehigh University, Bethlehem, Pennsylvania. 1989

Gere, J. M., and Timoshenko, S. P., *Mechanics of Materials.* Third Edition, PWS-KENT, Boston, Massachusetts. 1990.

Hallquist, J. O., *MAZE User's Manual.* Lawrence Livermore National Laboratory, Livermore, California. 1983

Hallquist, J. O., and Levatin, J. L., *ORION User's Manual.* Lawrence Livermore National Laboratory, Livermore, California. 1985.

LS-NIKE3D User's Manual. Version 970, Livermore Software Technology Corporation, Livermore, California. 1996.

"LS-TAURUS User's Manual: Appendix J," *LS-DYNA3D User's Manual*. Version 936, Livermore Software Technology Corporation, Livermore, California. 1995.

Maker, B. N., *NIKE3D User's Manual*. Lawrence Livermore National Laboratory, Livermore, California. 1991.

Marks, Lionel S., *Marks' Standard Handbook for Mechanical Engineers*. Tenth Edition, McGraw-Hill, Inc., New York, New York. 1996.

Moses, F., Schilling, C. G., and Raju K. S., *NCHRP Report 299 Fatigue Evaluation Procedures for Steel Bridges*. Transportation Research Board, Washington, DC. 1987.

Oregon Department of Transportation, *1994 Traffic Volume Tables*. Transportation Development Branch, Oregon Department of Transportation, Salem, Oregon. 1995

Shigley, J. E., and Mischke, C. R., *Mechanical Engineering Design*. Fifth Edition, McGraw-Hill, Inc., New York, New York. 1989

TrueGrid Manual. Version 0.99, XYZ Scientific Applications, Inc., Livermore, California. 1995.

Wilson, W. M., "Design of Connection Angles for Stringers of Railway Bridges." University of Illinois. 1940.

Wilson, W. M., and Coombe, J. V., "Fatigue Tests of Connection Angles." Engineering Experiment Station Bulletin Series No. 317, University of Illinois. 1939.

APPENDICES

APPENDIX A: STRINGER LOADING ANALYSIS
APPENDIX B: GLOBAL FEA MODEL
APPENDIX C: REINFORCED CONCRETE DECK ANALYSIS
APPENDIX D: CLIP ANGLE DEFLECTION ANALYSIS
APPENDIX E: CLIP ANGLE STRESS ANALYSIS
APPENDIX F: 2D FEA MODEL
APPENDIX G: 3D FEA MODEL
APPENDIX H: STRESS LIFE
APPENDIX I: LINEAR ELASTIC FRACTURE MECHANICS
APPENDIX J: IDENTIFICATION METHODOLOGY

NOTE: These Appendices may be obtained from the Oregon Department of Transportation Research Group, 200 Hawthorne Ave. SE, Suite B-240, Salem, OR 97301-5192. Telephone: 503-986-2700.